Journal of Sound and Vibration 573 (2024) 118199

Contents lists available at ScienceDirect

Journal of Sound and Vibration

journal homepage: www.elsevier.com/locate/jsvi

A multiple scattering formulation for elastic wave propagation in space–time modulated metamaterials

Xingbo Pu, Alessandro Marzani *, Antonio Palermo *

Department of Civil, Chemical, Environmental and Materials Engineering, University of Bologna, 40136 Bologna, Italy

ARTICLE INFO

Keywords:
Space–time modulation
Non-reciprocity
Metamaterials
Metasurfaces
One-way mode conversion

ABSTRACT

Space–time modulation of material parameters offers new possibilities for manipulating elastic wave propagation by exploiting time-reversal symmetry breaking. Here, we propose and validate a general framework based on the multiple scattering theory to model space–time modulated elastic metamaterials, namely elastic waveguides equipped with modulated resonators. The formulation allows to consider an arbitrary distribution of resonators with a generic space–time modulation profile and compute the wavefield within and outside the resonators' region. Under appropriate assumptions, the same framework can be exploited to predict the waveguide dispersion relation. We demonstrate the capabilities of our formulation by revisiting the dynamics of two representative space–time modulated systems, e.g., the non-reciprocal propagation of (i) flexural waves along a metabeam and (ii) surface acoustic waves along a metasurface. Given its flexibility, the proposed method can facilitate the design of novel devices able to realize unidirectional transport of elastic energy for vibration isolation, signal processing and energy harvesting purposes.

1. Introduction

In the last decade, the research on active (or activated) materials has fueled the discovery of novel dynamic functionalities to design devices for vibrations and waves control [1,2]. Active materials are often characterized by constitutive properties that are modulated in space and time according to an external energy source. The study of such space–time modulated materials was originally pioneered in optics [3] and, shortly afterward, extended to acoustics [4,5] and elasticity [1,6]. Elastic waves propagating in these space–time varying media are of particular interest since the modulation can create a directional bias that breaks the time-reversal symmetry. Breaking reciprocity allows to realize rich and unconventional phenomena, including, but not limited to, unidirectional wave propagation, adiabatic energy pumping [7,8], frequency conversion [9]. These effects can be leveraged to design novel devices such as acoustic rectifiers [10], circulators [11], and topological insulators [12], which can find applications in acoustic communication, signal processing, energy harvesting and vibration isolation [13–15].

In the context of elastodynamics, space–time modulation can be achieved by following two strategies. The first one relies on a bias directly introduced in the waveguide, as a modulation of the elastic and/or mass properties, so to obtain a modulated phononic crystal [16–18]. The second approach utilizes space–time modulated mechanical oscillators attached to a non-modulated waveguide [19–21] to obtain a modulated elastic metamaterial. Both strategies proved to be technically feasible by a series of experimental works where programmable electric components were used to modulate the media/oscillators [9,22–25]. Nonetheless, modulated metamaterials, compared to their phononic counterpart, are easier to realize, since only the resonant elements need to be modulated, and support non-reciprocal effects at sub-wavelength scales.

* Corresponding authors.
E-mail addresses: alessandro.marzani@unibo.it (A. Marzani), antonio.palermo6@unibo.it (A. Palermo).

https://doi.org/10.1016/j.jsv.2023.118199
Received 19 May 2023; Received in revised form 27 November 2023; Accepted 4 December 2023
Available online 6 December 2023

Besides the numerous examples of modulated waveguides [26,27], most of the conducted studies rely on the use of numerical simulations, typically developed via finite element (FE) or finite difference (FD) algorithms, to describe the expected non-reciprocal effects. Nonetheless, numerical simulations are always bounded by their computational cost which inherently limits the development of design and optimization studies. Computationally inexpensive analytical tools for modulated media are thus desirable, not only to reduce the computational burden but also to gain a deeper understanding of non-reciprocal effects. Currently, analytical formulations for time-modulated systems are mainly used to predict the dispersion relations of both discrete [28–30] and continuous media [17,19–24].

Although knowledge of the dispersion relations provides physical insights into the existence of directional band gaps, evidence of non-reciprocal phenomena can be found only by computing transient or steady-state responses across finite modulated systems. To the best of our knowledge, analytical methods for the computation of wavefields and transmission/reflection coefficients are currently limited to one-dimensional (1D) problems [18,22,31,32]. Additionally, there is no unified framework that enables the computation of both the dispersion relation and the wavefield of a generic modulated system.

To fill this gap, we propose a generalized multiple scattering formulation able to model the dynamic response of space–time modulated resonators coupled to a generic elastic waveguide. As observed in experiments, space–time modulated resonators can generate scattered fields at lower and higher harmonics with respect to the excitation frequency [22]. To capture this response, we first describe the coupling between the vibrating resonators and the waveguide motion with an ad-hoc impedance operator able to account for the expected additional harmonics. Then, we compute the scattered fields in the waveguide by means of Green's functions. Finally, we set our multiple scattering scheme to couple the incident and scattered fields and compute the related unknown amplitudes by imposing proper boundary conditions at each resonator base. The proposed formulation allows us to investigate the dynamic of an arbitrary number N of resonators with an arbitrary spatial–temporal modulation profile, since all the space–time varying oscillators can be described individually. Additionally, by introducing appropriate assumptions, the same formulation can be used to derive the related dispersion equations.

The details of the methodology and its modeling capabilities are discussed in what follows. In particular, in Section 2 we describe the proposed general multiple scattering formulation for the computation of the wavefield and the dispersion relation of waveguides coupled with space–time-modulated resonators. In Section 3, we apply the formulation to model flexural waves in a beam and Rayleigh waves on a substrate, both coupled with an array of modulated surface resonators. For both scenarios, we show the capability of the formulation to predict non-reciprocal guided waves. Finally, we derive conclusions and outlook of the work in Section 4.

2. Theoretical formulation

2.1. Statement of the problem

We propose a general analytical framework to model a cluster of space–time-modulated oscillators attached to a given elastic waveguide (Fig. 1). The formulation includes the following three steps: (i) the definition of the elastic force exerted on the waveguide by a time-modulated resonator when excited by a base motion; (ii) the use of Green's functions to describe the scattered wavefields generated by the resonators in the waveguide; (iii) the construction of a multiple scattering formulation to couple the waveguide with an arbitrary number of time-modulated resonators. The approach allows computing the lower- and higher-order scattered harmonics, generated by the collective response of the time-modulated resonators, and responsible for the non-reciprocal wave motion in the waveguide.

First, we present the framework in its most general form, i.e. considering a finite array of time-modulated oscillators with mechanical properties obeying the same modulation period T_m and arbitrarily arranged over the waveguide surface. Then, we show how to derive the waveguide dispersion relation by introducing appropriate assumptions, e.g., considering an infinite array of identical resonators regularly arranged along the elastic support.

2.2. Elastic force of a time-modulated resonator

Let us recall the dynamics of the generic nth resonator attached to the waveguide surface at the location $\mathbf{r}_n$ (see Fig. 1). The resonator has a mass m_n, damping coefficient c_n, and time-modulated spring stiffness $k_n(t)$:

$$k_n(t) = k_n(t + T_m), \tag{1}$$

where T_m is the modulation time period. The governing equation of the nth resonator motion reads:

$$m_n \frac{\partial^2 W_n(t)}{\partial t^2} + c_n \left[\frac{\partial W_n(t)}{\partial t} - \frac{\partial w_n(t)}{\partial t} \right] + k_n(t)[W_n(t) - w_n(t)] = 0, \tag{2}$$

in which $W_n(t) = W(\mathbf{r}_n, t)$ denotes the mass vertical displacement while $w_n(t) = w(\mathbf{r}_n, t)$ is the vertical motion at the resonator base. Accordingly, the point force $F_n(t) = F(\mathbf{r}_n, t)$ exerted by the resonator onto the waveguide surface reads:

$$F_n(t) = -m_n \frac{\partial^2 W_n(t)}{\partial t^2}. \tag{3}$$

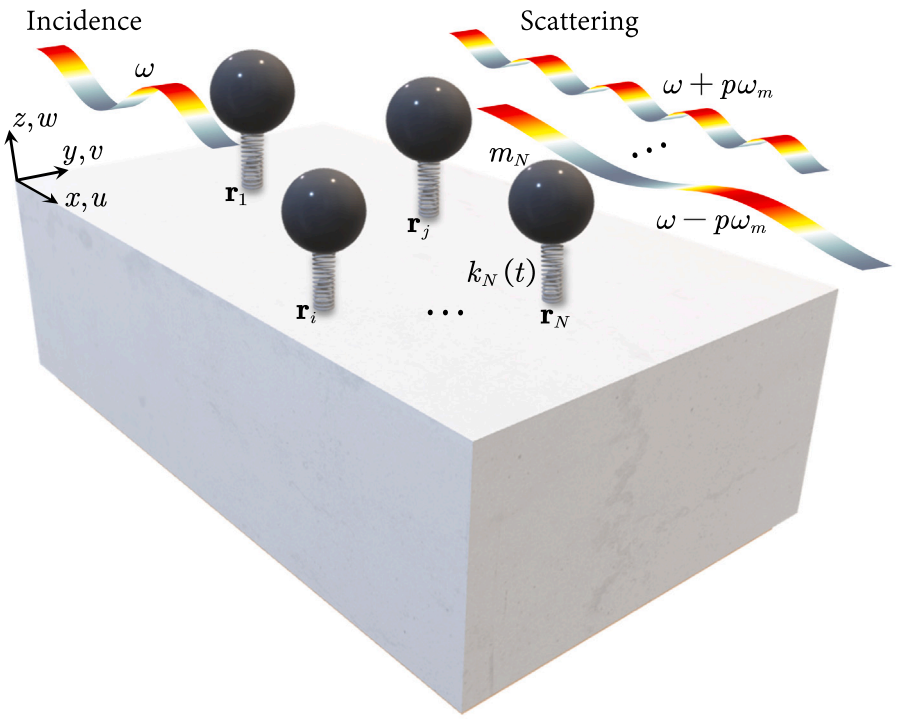

Fig. 1. Schematics of space–time modulated resonators laying over an elastic waveguide.

Since the modulated stiffness $k_n(t)$ in Eq. (1) is time-periodic, we express it in Fourier series form as:

$$k_n(t) = \sum_{j=-\infty}^{\infty} \hat{k}_n^{(j)} \mathrm{e}^{\mathrm{i}j\omega_m t}, \quad j \in \mathbb{Z}, \tag{4}$$

in which $\mathrm{i} = \sqrt{-1}$ is the imaginary unit, $\omega_m = 2\pi/T_m$ is the modulation frequency, and where the Fourier coefficients are defined as:

$$\hat{k}_n^{(j)} = \frac{\omega_m}{2\pi} \int_{\frac{-\pi}{\omega_m}}^{\frac{\pi}{\omega_m}} k_n(t) \mathrm{e}^{-\mathrm{i}j\omega_m t} \, \mathrm{d}t. \tag{5}$$

As we will see in the next section, the motion along the waveguide excited by a harmonic ($\mathrm{e}^{\mathrm{i}\omega t}$) incident field, contains several lower- and higher-order harmonics generated by the scattering of the time-modulated mechanical resonators. As a result, the vertical motion at the resonator base, namely the motion at the waveguide surface, can be written as [31]:

$$w_n(t) = \sum_{h=-\infty}^{\infty} \hat{w}_n^{(h)} \mathrm{e}^{\mathrm{i}(\omega + h\omega_m)t}, \quad h \in \mathbb{Z}, \tag{6}$$

so that the solution of Eq. (2) is sought in the form [18,22,23]:

$$W_n(t) = \sum_{h=-\infty}^{\infty} \hat{W}_n^{(h)} \mathrm{e}^{\mathrm{i}(\omega + h\omega_m)t}, \quad h \in \mathbb{Z}. \tag{7}$$

Substituting Eqs. (4), (6) and (7) into Eq. (2), yields:

$$\begin{aligned} &\sum_{h=-\infty}^{\infty} [-m_n(\omega + h\omega_m)^2 + \mathrm{i}c_n(\omega + h\omega_m)] \hat{W}_n^{(h)} \mathrm{e}^{\mathrm{i}h\omega_m t} + \sum_{h=-\infty}^{\infty} \sum_{j=-\infty}^{\infty} \hat{k}_n^{(j)} \hat{W}_n^{(h)} \mathrm{e}^{\mathrm{i}(j+h)\omega_m t} \\ &= \sum_{h=-\infty}^{\infty} \mathrm{i}c_n(\omega + h\omega_m) \hat{w}_n^{(h)} \mathrm{e}^{\mathrm{i}h\omega_m t} + \sum_{h=-\infty}^{\infty} \sum_{j=-\infty}^{\infty} \hat{k}_n^{(j)} \hat{w}_n^{(h)} \mathrm{e}^{\mathrm{i}(j+h)\omega_m t}. \end{aligned} \tag{8}$$

Exploiting the orthogonality of harmonic functions, we simplify Eq. (8) by multiplying it for $\omega_m \mathrm{e}^{-\mathrm{i}p\omega_m t}/(2\pi)$, and integrating it from $-\pi/\omega_m$ to π/ω_m, to obtain:

$$[-m_n(\omega + p\omega_m)^2 + \mathrm{i}c_n(\omega + p\omega_m)] \hat{W}_n^{(p)} + \sum_{j=-\infty}^{\infty} \hat{k}_n^{(j)} \hat{W}_n^{(p-j)} = \mathrm{i}c_n(\omega + p\omega_m) \hat{w}_n^{(p)} + \sum_{j=-\infty}^{\infty} \hat{k}_n^{(j)} \hat{w}_n^{(p-j)}, \quad p \in \mathbb{Z}. \tag{9}$$

By truncating the orders from $-P$ to P, Eq. (9) can be reorganized in matrix form as:

$$\mathbf{M}_n\hat{\mathbf{W}}_n = \mathbf{Q}_n\hat{\mathbf{w}}_n, \tag{10}$$

with:

$$\mathbf{M}_n = \begin{bmatrix} \hat{m}_n^{(-P)} & \hat{k}_n^{(-1)} & \hat{k}_n^{(-2)} & \cdots & \hat{k}_n^{(-2P)} \\ \hat{k}_n^{(1)} & \hat{m}_n^{(-P+1)} & \hat{k}_n^{(-1)} & \cdots & \hat{k}_n^{(-2P+1)} \\ \hat{k}_n^{(2)} & \hat{k}_n^{(1)} & \hat{m}_n^{(-P+2)} & \cdots & \hat{k}_n^{(-2P+2)} \\ \vdots & \vdots & \vdots & \ddots & \vdots \\ \hat{k}_n^{(2P)} & \hat{k}_n^{(2P-1)} & \hat{k}_n^{(2P-2)} & \cdots & \hat{m}_n^{(P)} \end{bmatrix}, \mathbf{Q}_n = \begin{bmatrix} \hat{q}_n^{(-P)} & \hat{k}_n^{(-1)} & \hat{k}_n^{(-2)} & \cdots & \hat{k}_n^{(-2P)} \\ \hat{k}_n^{(1)} & \hat{q}_n^{(-P+1)} & \hat{k}_n^{(-1)} & \cdots & \hat{k}_n^{(-2P+1)} \\ \hat{k}_n^{(2)} & \hat{k}_n^{(1)} & \hat{q}_n^{(-P+2)} & \cdots & \hat{k}_n^{(-2P+2)} \\ \vdots & \vdots & \vdots & \ddots & \vdots \\ \hat{k}_n^{(2P)} & \hat{k}_n^{(2P-1)} & \hat{k}_n^{(2P-2)} & \cdots & \hat{q}_n^{(P)} \end{bmatrix},$$
$$\hat{\mathbf{W}}_n = [\hat{W}_n^{(-P)}, \hat{W}_n^{(-P+1)}, \ldots, \hat{W}_n^{(P-1)}, \hat{W}_n^{(P)}]^T, \quad \hat{\mathbf{w}}_n = [i\hat{w}_n^{(-P)}, i\hat{w}_n^{(-P+1)}, \ldots, i\hat{w}_n^{(P-1)}, i\hat{w}_n^{(P)}]^T, \tag{11}$$

in which $\hat{m}_n^{(j)} = \hat{k}_n^{(0)} - m_n(\omega + j\omega_m)^2 + \mathrm{i}c_n(\omega + j\omega_m)$, and $\hat{q}_n^{(j)} = \hat{k}_n^{(0)} + \mathrm{i}c_n(\omega + j\omega_m)$.

The vertical force at the base of the resonator can thus be obtained by substituting Eq. (7) into Eq. (3):

$$F_n(t) = -m_n\frac{\partial^2}{\partial t^2}\sum_{h=-\infty}^{\infty}\hat{W}_n^{(h)}\mathrm{e}^{\mathrm{i}(\omega+h\omega_m)t} = m_n\sum_{h=-\infty}^{\infty}(\omega+h\omega_m)^2\hat{W}_n^{(h)}\mathrm{e}^{\mathrm{i}(\omega+h\omega_m)t} = \sum_{h=-\infty}^{\infty}\hat{F}_n^{(h)}\mathrm{e}^{\mathrm{i}(\omega+h\omega_m)t}, \quad h\in\mathbb{Z}, \tag{12}$$

where the $\hat{F}_n^{(h)}$ coefficients from $h=-P$ to $h=P$, collected in the vector $\hat{\mathbf{F}}_n$, read:

$$\hat{\mathbf{F}}_n = \mathbf{D}_n\hat{\mathbf{W}}_n = \mathbf{D}_n\mathbf{M}_n^{-1}\mathbf{Q}_n\hat{\mathbf{w}}_n =: \mathbf{Z}_n\hat{\mathbf{w}}_n, \tag{13}$$

with:

$$\hat{\mathbf{F}}_n = \begin{bmatrix} \hat{F}_n^{(-P)} \\ \hat{F}_n^{(-P+1)} \\ \vdots \\ \hat{F}_n^{(P)} \end{bmatrix}, \mathbf{D}_n = \begin{bmatrix} m_n(\omega - P\omega_m)^2 & 0 & \cdots & 0 \\ 0 & m_n[\omega + (-P+1)\omega_m]^2 & \cdots & 0 \\ \vdots & \vdots & \ddots & \vdots \\ 0 & 0 & \cdots & m_n(\omega + P\omega_m)^2 \end{bmatrix}. \tag{14}$$

In Eq. (13), the matrix $\mathbf{Z}_n$ is the impedance operator which relates the resonator base motion to the resonator base force. It can be observed that the force exerted by each modulated resonator on the elastic substrate comprises multiple harmonics $(\omega + h\omega_m)$. In the next section, we discuss how these forces generate the related multiple scattered wavefields.

2.3. Elastic wave field of a finite cluster of modulated resonators

We now consider an arbitrary distribution of N space–time modulated resonators arranged on top of a given elastic waveguide. We assume that the resonators have an identical stiffness modulation frequency ω_m. When an incident wave field $\mathbf{u}_0 = [u_0, v_0, w_0]$ impinges the bases of such resonators, it triggers their vibrations which, in turn, generate scattered waves in the waveguide. Following a standard multiple scattering description [33–39], the total wave field $\mathbf{u} = (u, v, w)$ at the generic position $\mathbf{r}$ along the waveguide can be expressed as the summation of the incident and scattered wave fields of the N resonators:

$$u(\mathbf{r},t) = u_0(\mathbf{r},t) + \sum_{n=1}^{N}F_n(t)G_u(\mathbf{r}-\mathbf{r}_n), \tag{15a}$$

$$v(\mathbf{r},t) = v_0(\mathbf{r},t) + \sum_{n=1}^{N}F_n(t)G_v(\mathbf{r}-\mathbf{r}_n), \tag{15b}$$

$$w(\mathbf{r},t) = w_0(\mathbf{r},t) + \sum_{n=1}^{N}F_n(t)G_w(\mathbf{r}-\mathbf{r}_n), \tag{15c}$$

where G_u, G_v, G_w are the related Green's functions in terms of displacements along x, y, z. As in the previous section, we express the displacements of Eqs. (15a), (15b), (15c) accounting for the multiple harmonics:

$$\sum_{h=-\infty}^{\infty}\hat{u}^{(h)}(\mathbf{r})\mathrm{e}^{\mathrm{i}(\omega+h\omega_m)t} = \sum_{h=-\infty}^{\infty}\hat{u}_0^{(h)}(\mathbf{r})\mathrm{e}^{\mathrm{i}(\omega+h\omega_m)t} + \sum_{n=1}^{N}\sum_{h=-\infty}^{\infty}\hat{F}_n^{(h)}\hat{G}_u^{(h)}(\mathbf{r}-\mathbf{r}_n,\omega+h\omega_m)\mathrm{e}^{\mathrm{i}(\omega+h\omega_m)t}, \quad h\in\mathbb{Z}. \tag{16a}$$

$$\sum_{h=-\infty}^{\infty}\hat{v}^{(h)}(\mathbf{r})\mathrm{e}^{\mathrm{i}(\omega+h\omega_m)t} = \sum_{h=-\infty}^{\infty}\hat{v}_0^{(h)}(\mathbf{r})\mathrm{e}^{\mathrm{i}(\omega+h\omega_m)t} + \sum_{n=1}^{N}\sum_{h=-\infty}^{\infty}\hat{F}_n^{(h)}\hat{G}_v^{(h)}(\mathbf{r}-\mathbf{r}_n,\omega+h\omega_m)\mathrm{e}^{\mathrm{i}(\omega+h\omega_m)t}, \quad h\in\mathbb{Z}. \tag{16b}$$

$$\sum_{h=-\infty}^{\infty}\hat{w}^{(h)}(\mathbf{r})\mathrm{e}^{\mathrm{i}(\omega+h\omega_m)t} = \sum_{h=-\infty}^{\infty}\hat{w}_0^{(h)}(\mathbf{r})\mathrm{e}^{\mathrm{i}(\omega+h\omega_m)t} + \sum_{n=1}^{N}\sum_{h=-\infty}^{\infty}\hat{F}_n^{(h)}\hat{G}_w^{(h)}(\mathbf{r}-\mathbf{r}_n,\omega+h\omega_m)\mathrm{e}^{\mathrm{i}(\omega+h\omega_m)t}, \quad h\in\mathbb{Z}. \tag{16c}$$

Truncating the harmonic terms from $h=-P$ to $h=P$, Eqs. (16a), (16b), (16c) can be rewritten as:

$$\hat{\mathbf{u}}(\mathbf{r}) = \hat{\mathbf{u}}_0(\mathbf{r}) + \sum_{n=1}^{N}\hat{\mathbf{G}}_u(\mathbf{r}-\mathbf{r}_n)\hat{\mathbf{F}}_n, \tag{17a}$$

$$\hat{\mathbf{v}}(\mathbf{r}) = \hat{\mathbf{v}}_0(\mathbf{r}) + \sum_{n=1}^{N} \hat{\mathbf{G}}_v(\mathbf{r}-\mathbf{r}_n)\hat{\mathbf{F}}_n, \tag{17b}$$

$$\hat{\mathbf{w}}(\mathbf{r}) = \hat{\mathbf{w}}_0(\mathbf{r}) + \sum_{n=1}^{N} \hat{\mathbf{G}}_w(\mathbf{r}-\mathbf{r}_n)\hat{\mathbf{F}}_n, \tag{17c}$$

with:

$$\hat{\boldsymbol{\varphi}}(\mathbf{r}) = \begin{bmatrix} \hat{\varphi}^{(-P)}(\mathbf{r}) \\ \hat{\varphi}^{(-P+1)}(\mathbf{r}) \\ \vdots \\ \hat{\varphi}^{(P)}(\mathbf{r}) \end{bmatrix}, \quad \hat{\boldsymbol{\varphi}}_0(\mathbf{r}) = \begin{bmatrix} \hat{\varphi}_0^{(-P)}(\mathbf{r}) \\ \hat{\varphi}_0^{(-P+1)}(\mathbf{r}) \\ \vdots \\ \hat{\varphi}_0^{(P)}(\mathbf{r}) \end{bmatrix}, \quad \varphi = u, v, w.$$

$$\hat{\mathbf{G}}_\varphi(\mathbf{r}-\mathbf{r}_n) = \begin{bmatrix} \hat{G}_\varphi^{(-P)}(\mathbf{r}-\mathbf{r}_n, \omega - P\omega_m) & 0 & \cdots & 0 \\ 0 & \hat{G}_\varphi^{(-P+1)}(\mathbf{r}-\mathbf{r}_n, \omega - P\omega_m + \omega_m) & \cdots & 0 \\ \vdots & \vdots & \ddots & \vdots \\ 0 & 0 & \cdots & \hat{G}_\varphi^{(P)}(\mathbf{r}-\mathbf{r}_n, \omega + P\omega_m) \end{bmatrix},$$

and where $\hat{\boldsymbol{\varphi}}_0$ has non-zero components only for the incident field $\varphi_0 = u_0, v_0, w_0$:

$$\hat{\varphi}_0^{(j)} = \begin{cases} \varphi_0 & j = 0 \\ 0 & j \neq 0 \end{cases}, \quad j \in [-P, -P+1, \dots, P] \tag{18}$$

Note that in Eqs. (17a), (17b), (17c) the total displacement components $\hat{\mathbf{u}}, \hat{\mathbf{v}}, \hat{\mathbf{w}}$ and the elastic force coefficients $\hat{\mathbf{F}}_n$ are unknown. Nonetheless, following a classical multiple scattering approach, we can obtain the coefficients $\hat{\mathbf{F}}_n$ by setting boundary conditions at resonator bases. In particular, we substitute Eq. (13) into Eq. (17c) and specify it at the resonator location $\mathbf{r}_m$:

$$\mathbf{Z}_m^{-1}\hat{\mathbf{F}}_m = \hat{\mathbf{w}}_0(\mathbf{r}_m) + \sum_{n=1}^{N} \hat{\mathbf{G}}_w(\mathbf{r}_m-\mathbf{r}_n)\hat{\mathbf{F}}_n, \quad n, m = 1, \dots, N. \tag{19}$$

Eq. (19) leads to a system of $m = N$ equations that we can recast in matrix form as:

$$\mathbf{A}\mathbf{X} = \mathbf{B}, \tag{20}$$

with:

$$\mathbf{A} = \begin{bmatrix} \mathbf{Z}_1^{-1} - \hat{\mathbf{G}}_w(\mathbf{0}) & -\hat{\mathbf{G}}_w(\mathbf{r}_1-\mathbf{r}_2) & \cdots & -\hat{\mathbf{G}}_w(\mathbf{r}_1-\mathbf{r}_N) \\ -\hat{\mathbf{G}}_w(\mathbf{r}_2-\mathbf{r}_1) & \mathbf{Z}_2^{-1} - \hat{\mathbf{G}}_w(\mathbf{0}) & \cdots & -\hat{\mathbf{G}}_w(\mathbf{r}_2-\mathbf{r}_N) \\ \vdots & \vdots & \ddots & \vdots \\ -\hat{\mathbf{G}}_w(\mathbf{r}_N-\mathbf{r}_1) & -\hat{\mathbf{G}}_w(\mathbf{r}_N-\mathbf{r}_2) & \cdots & \mathbf{Z}_N^{-1} - \hat{\mathbf{G}}_w(\mathbf{0}) \end{bmatrix}, \quad \mathbf{X} = \begin{bmatrix} \hat{\mathbf{F}}_1 \\ \hat{\mathbf{F}}_2 \\ \vdots \\ \hat{\mathbf{F}}_N \end{bmatrix}, \quad \mathbf{B} = \begin{bmatrix} \hat{\mathbf{w}}_0(\mathbf{r}_1) \\ \hat{\mathbf{w}}_0(\mathbf{r}_2) \\ \vdots \\ \hat{\mathbf{w}}_0(\mathbf{r}_N) \end{bmatrix}. \tag{21}$$

It follows that for a given incident wave field $\hat{\mathbf{w}}_0$, the vector $\mathbf{X}$ of the force amplitudes $\hat{\mathbf{F}}_n$ can be computed as $\mathbf{X} = \mathbf{A}^{-1}\mathbf{B}$, and the total wave field in the waveguide evaluated by using Eqs. (15a), (15b), (15c).

In addition, we will show in the following subsection that Eq. (20), under appropriate assumptions, allows to derive the dispersion relation of time-modulated waveguides.

2.4. Dispersion relation

We here consider an infinite array of equally spaced resonators, arranged atop an elastic waveguide (see Fig. 2) at lattice distance a. We restrict our interest to oscillators with identical mass and with spring constant modulated in time and space with a wave-like modulation of period $T_m = 2\pi/\omega_m$ and wavelength $\lambda_m = 2\pi/\kappa_m$, whose general form reads:

$$k(x,t) = k(x+\lambda_m, t+T_m). \tag{22}$$

As before, we express $k(x,t)$ in a Fourier series form:

$$k(x,t) = \sum_{j=-\infty}^{\infty} \hat{k}^{(j)} \mathrm{e}^{\mathrm{i}j(\omega_m t - \kappa_m x)}, \quad j \in \mathbb{Z}, \tag{23}$$

where the Fourier coefficients are computed as:

$$\hat{k}^{(j)} = \frac{\kappa_m}{2\pi}\frac{\omega_m}{2\pi}\int_{\frac{-\pi}{\kappa_m}}^{\frac{\pi}{\kappa_m}}\int_{\frac{-\pi}{\omega_m}}^{\frac{\pi}{\omega_m}} k(x,t)\mathrm{e}^{-\mathrm{i}j(\omega_m t - \kappa_m x)}\,\mathrm{d}x\mathrm{d}t. \tag{24}$$

As discussed in [21,31], a stable response of the modulated system requires each modulation amplitude $\hat{k}^{(j)} (j \neq 0)$ to be sufficiently small with respect to the static stiffness $\hat{k}^{(0)}$. Under this assumption, for the assumed infinite ($N \to \infty$) periodic array of identical resonators, the scattering Eqs. (19) are the same at any location x_m and satisfy:

$$\mathbf{Z}^{-1}\hat{\mathbf{F}} = \sum_{n=-N}^{N} \hat{\mathbf{G}}_w(x_n)\hat{\mathbf{F}}(x_n) = \sum_{n=-\infty}^{\infty} \hat{\mathbf{G}}_w(x_n)\hat{\mathbf{F}}(x_n) \tag{25}$$

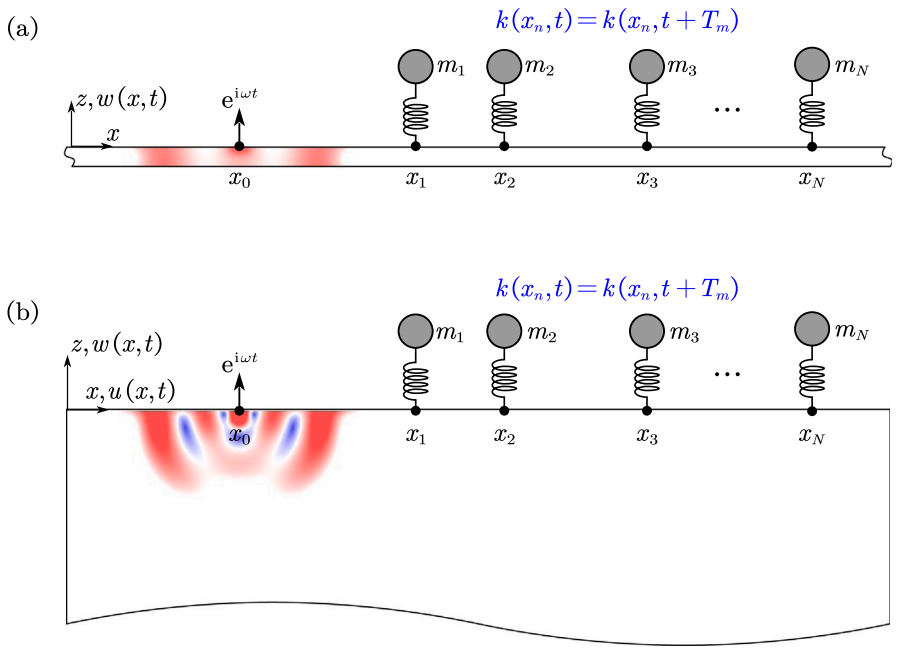

Fig. 2. Schematic of wave propagation in space–time modulated (a) metabeam and (b) metasurface.

where x_m has been conveniently set equal to 0.

Following the effective medium approach [40–42], namely considering the lattice spacing a much smaller than the characteristic wavelength, we approximate the discrete point force as an average line load. As a result, the total vertical displacement at the generic resonator base can be computed as:

$$\mathbf{Z}^{-1}\hat{\mathbf{F}} = \frac{1}{a}\sum_{n=-\infty}^{\infty}\int_{x_n-a/2}^{x_n+a/2}\hat{\mathbf{G}}_w(x)\hat{\mathbf{F}}(x)\,\mathrm{d}x = \frac{1}{a}\int_{-\infty}^{\infty}\hat{\mathbf{G}}_w(x)\hat{\mathbf{F}}(x)\,\mathrm{d}x. \tag{26}$$

Due to the space–time modulation of the resonator properties, we can express the force in Eq. (12) in the form:

$$F(x,t) = \sum_{h=-\infty}^{\infty}\hat{F}^{(h)}\mathrm{e}^{-\mathrm{i}(\kappa+h\kappa_m)x+\mathrm{i}(\omega+h\omega_m)t}, \quad h\in\mathbb{Z}. \tag{27}$$

Substituting Eq. (27) into Eq. (26) and truncating the orders from $h=-P$ to $h=P$ we obtain:

$$a\mathbf{Z}^{-1}\begin{bmatrix}\hat{F}^{(-P)}\\ \hat{F}^{(-P+1)}\\ \vdots\\ \hat{F}^{(P)}\end{bmatrix} = \int_{-\infty}^{\infty}\begin{bmatrix}\hat{G}_w^{(-P)}(x,\omega-P\omega_m) & 0 & \cdots & 0\\ 0 & \hat{G}_w^{(-P+1)}(x,\omega-P\omega_m+\omega_m) & \cdots & 0\\ \vdots & \vdots & \ddots & \vdots\\ 0 & 0 & \cdots & \hat{G}_w^{(P)}(x,\omega+P\omega_m)\end{bmatrix}\begin{bmatrix}\hat{F}^{(-P)}\mathrm{e}^{-\mathrm{i}(\kappa-P\kappa_m)x}\\ \hat{F}^{(-P+1)}\mathrm{e}^{-\mathrm{i}(\kappa-P\kappa_m+\kappa_m)x}\\ \vdots\\ \hat{F}^{(P)}\mathrm{e}^{-\mathrm{i}(\kappa+P\kappa_m)x}\end{bmatrix}\mathrm{d}x. \tag{28}$$

Some minor algebra yields the following system of homogeneous equations:

$$\left(a\mathbf{Z}^{-1}-\begin{bmatrix}\tilde{\mathbf{G}}(\kappa-P\kappa_m,\omega-P\omega_m) & 0 & \cdots & 0\\ 0 & \tilde{\mathbf{G}}(\kappa-P\kappa_m+\kappa_m,\omega-P\omega_m+\omega_m) & \cdots & 0\\ \vdots & \vdots & \ddots & \vdots\\ 0 & 0 & \cdots & \tilde{\mathbf{G}}(\kappa+P\kappa_m,\omega+P\omega_m)\end{bmatrix}\right)\begin{bmatrix}\hat{F}^{(-P)}\\ \hat{F}^{(-P+1)}\\ \vdots\\ \hat{F}^{(P)}\end{bmatrix} = \mathbf{0}, \tag{29}$$

in which $\tilde{\mathbf{G}}(\kappa+P\kappa_m,\omega+P\omega_m)$ is Pth order Green's function in space-domain which is obtained as:

$$\int_{-\infty}^{\infty}\hat{G}_w^{(P)}(x,\omega+P\omega_m)\mathrm{e}^{-\mathrm{i}(\kappa+P\kappa_m)x}\,\mathrm{d}x = \tilde{\mathbf{G}}(\kappa+P\kappa_m,\omega+P\omega_m). \tag{30}$$

Non-trivial solutions of Eq. (29) provide the dispersion relation:

$$\tilde{C}(\kappa,\omega) := \left| a\mathbf{Z}^{-1} - \begin{bmatrix} \tilde{\mathbf{G}}(\kappa - P\kappa_m, \omega - P\omega_m) & 0 & \cdots & 0 \\ 0 & \tilde{\mathbf{G}}(\kappa - P\kappa_m + \kappa_m, \omega - P\omega_m + \omega_m) & \cdots & 0 \\ \vdots & \vdots & \ddots & \vdots \\ 0 & 0 & \cdots & \tilde{\mathbf{G}}(\kappa + P\kappa_m, \omega + P\omega_m) \end{bmatrix} \right| = 0. \tag{31}$$

3. Examples and applications

To show the capabilities of our formulation, we consider two space–time-modulated waveguides that have been thoroughly discussed in previous works [19–22]. We begin our investigation by considering an Euler beam coupled with an array of modulated resonators. For this example, we validate our approach against the results of the Transfer Matrix Method (TMM). For the sake of completeness we report in Appendix A the full derivation of the adopted TMM [22]. As a second example, we consider a 2D elastic half-space coupled to modulated resonators. For this configuration, given the absence of closed-form formulations, we compare our findings vs. those obtained via finite element simulations, as in Ref. [21].

3.1. Modeling non-reciprocal flexural waves in a space–time modulated beam

We consider an Euler–Bernoulli beam equipped with an array of undamped resonators, see Fig. 2a, modulated in a wave-like fashion according to the relationship [19,22,28,29]:

$$k(t,x) = k_0 + k_a \cos(\omega_m t - \kappa_m x), \tag{32}$$

where k_0 denotes the static stiffness, k_a the amplitude of the modulation, ω_m the modulation angular frequency, κ_m the modulation wavenumber. At any location x_n, the modulated stiffness is time-periodic and its non-zero Fourier coefficients read:

$$\hat{k}_n^{(0)} = k_0, \quad \hat{k}_n^{(-1)} = \frac{1}{2} k_a \mathrm{e}^{\mathrm{i}\kappa_m x_n}, \quad \hat{k}_n^{(1)} = \frac{1}{2} k_a \mathrm{e}^{-\mathrm{i}\kappa_m x_n}, \tag{33}$$

as $\hat{k}_n^{(j)} = 0$ for $|j| > 1$. For the numerical example, we consider the mechanical parameters originally adopted in Ref. [19], i.e., a resonator mass $m_0 = \rho \mathcal{A} a$, where ρ is the mass density of the beam and $\mathcal{A}$ is the cross-section area of the beam. Similarly, the modulation frequency is set as $\omega_m = 0.25\omega_0$ and modulation amplitude as $k_a = 0.2k_0$, in which ω_0 is the resonance frequency of resonators and $k_0 = m_0\omega_0^2$ is the unmodulated stiffness; the modulation wavenumber is $\kappa_m = 1.25\kappa_0$, where $\kappa_0 = \sqrt[4]{k_0/(aD)}$, D the bending stiffness of the beam.

3.1.1. Dispersion relation

According to the Euler–Bernoulli beam theory, the Pth order governing equation under the action of a harmonic point force can be written as:

$$D\frac{\partial^4 w}{\partial x^4} + \rho\mathcal{A}\frac{\partial^2 w}{\partial t^2} = \delta(x)\,\mathrm{e}^{\mathrm{i}\omega_P t}, \quad P \in \mathbb{Z}. \tag{34}$$

We Fourier transform Eq. (34) along the x direction, and obtain the transformed Pth order Green's function in space-domain as:

$$\tilde{G}(\kappa_P, \omega_P) = \frac{1}{D\kappa_P^4 - \rho\mathcal{A}\omega_P^2}, \tag{35}$$

where the shifted frequency and wavenumber are defined as:

$$\omega_P = \omega + P\omega_m, \quad \kappa_P = \kappa + P\kappa_m, \quad P \in \mathbb{Z}. \tag{36}$$

First, by setting $P = 0$ we get the non-modulated impedance parameter Z from Eq. (13) as:

$$Z = \frac{m_0\omega_0^2\omega^2}{\omega_0^2 - \omega^2}. \tag{37}$$

Substituting Eqs. (35) and (37) into Eq. (31) we obtain immediately the dispersion relation of a non-modulated metabeam:

$$C(\kappa,\omega) := D\kappa^4 - \left(\rho\mathcal{A} + \frac{m_0}{a}\frac{1}{1 - \omega^2/\omega_0^2}\right)\omega^2 = 0. \tag{38}$$

This dispersion equation is identical to the one obtained in Refs. [19,22] and matches the dispersion curve provided by FE simulations, see Appendix B for details.

In the presence of modulation, scattered waves are expected when the phase matching condition is satisfied, i.e., $C(\kappa,\omega) = C(\kappa_P,\omega_P)$ [29]. As an example, in Fig. 3a we show the original (C) and the two shifted dispersion curves ($C^{\pm 1}$) for $P = \pm 1$, respectively. The phase matching condition is met at the intersections between the original curve and the shifted ones, namely at the six magenta points marking the pairs (A), (B) and (C). The asymmetric distribution of these intersections suggests the breaking of time-reversal symmetry which, in turn, leads to direction-dependent phenomena within the metabeam [22].

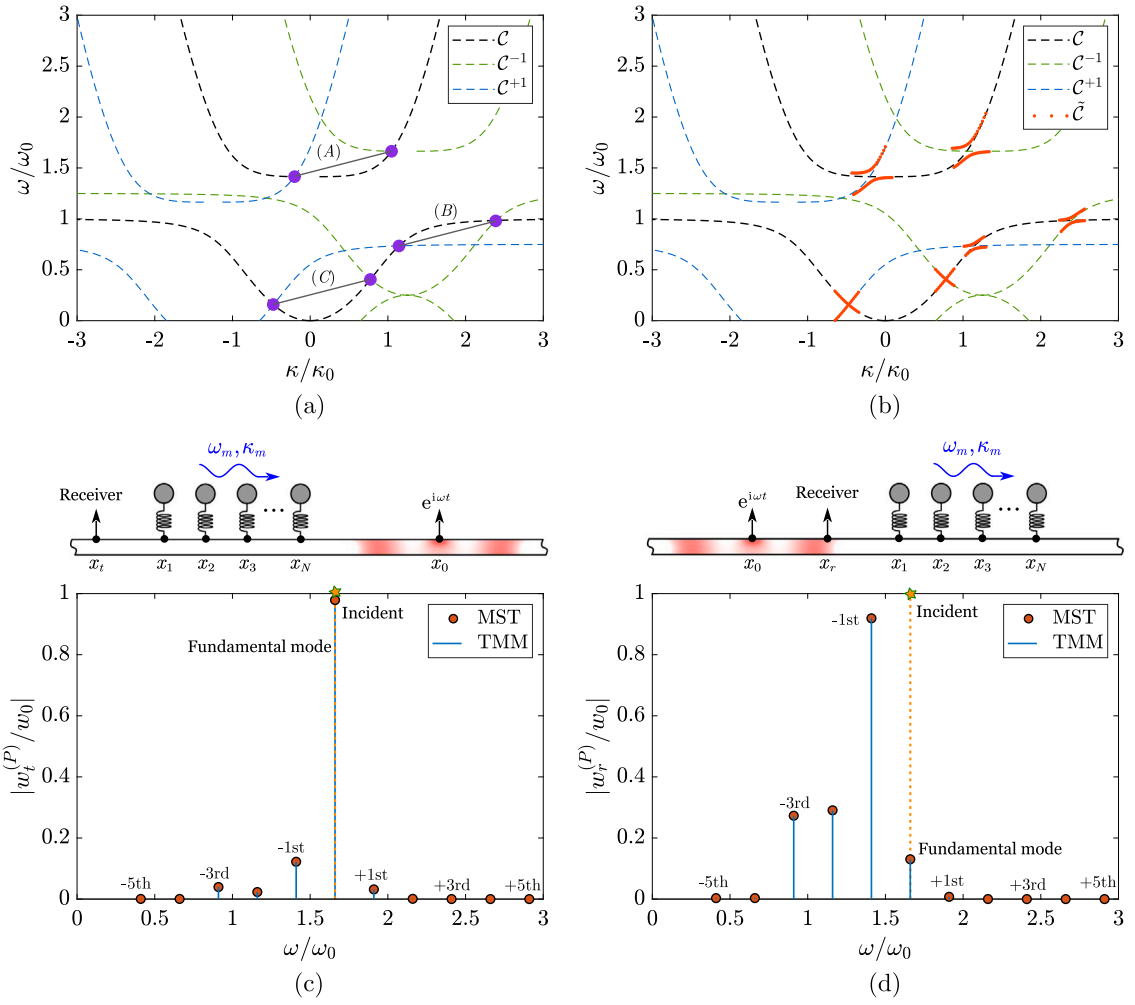

Fig. 3. (a) Dispersion curve of a non-modulated metabeam (black dashed lines) and its shifted analogs for $P = -1$ and $P = 1$, respectively. (b) Dispersion curves (circular red markers) of a modulated metabeam in the proximity of the phase-matching pairs. Normalized transmission and reflection coefficients for flexural waves propagating at $\omega = 1.66\omega_0$ inside the directional band gap (pair A) for (c) a left and (d) a right traveling incident wave (star marker), respectively. For comparison, results obtained by the transfer matrix method (TMM) are also provided (blue solid lines). (For interpretation of the references to color in this figure legend, the reader is referred to the web version of this article.)

We now predict the dispersion properties of the modulated metabeam. To this purpose, we substitute Eq. (35) into Eq. (31) by truncating waves to the first order ($P = 1$), which yields:

$$\tilde{C}(\kappa,\omega) := \left| a\mathbf{Z}^{-1} - \begin{bmatrix} 1/[D(\kappa-\kappa_m)^4 - \rho\mathcal{A}(\omega-\omega_m)^2] & 0 & 0 \\ 0 & 1/[D\kappa^4 - \rho\mathcal{A}\omega^2] & 0 \\ 0 & 0 & 1/[D(\kappa+\kappa_m)^4 - \rho\mathcal{A}(\omega+\omega_m)^2] \end{bmatrix} \right| = 0, \tag{39}$$

with the impedance operator:

$$\mathbf{Z} = m_0 \begin{bmatrix} (\omega-\omega_m)^2 & 0 & 0 \\ 0 & \omega^2 & 0 \\ 0 & 0 & (\omega+\omega_m)^2 \end{bmatrix} \begin{bmatrix} k_0 - m_0(\omega-\omega_m)^2 & 0.5k_a & 0 \\ 0.5k_a & k_0 - m_0\omega^2 & 0.5k_a \\ 0 & 0.5k_a & k_0 - m_0(\omega+\omega_m)^2 \end{bmatrix}^{-1} \begin{bmatrix} k_0 & 0.5k_a & 0 \\ 0.5k_a & k_0 & 0.5k_a \\ 0 & 0.5k_a & k_0 \end{bmatrix}. \tag{40}$$

We remark that the coupled dispersion relation in Eq. (39) holds only near the above-mentioned intersections in Fig. 3a [30]. Thus, we compute and plot the coupled dispersion in the range of $\pm 0.1\kappa$ and $\pm 0.1\omega$ around each crossing point, as shown in Fig. 3b (red circular markers). For comparison, we also provide the unmodulated dispersion curve (solution of Eq. (38)) and its shifted analogs on the same figure. As discussed in Ref. [19], in the vicinity of pair B no directional band gap is generated, since both modes have positive group velocities. Conversely, for contra-directional branches such as pairs A and C, the repulsion effect

between the branches can lead to narrow band directional gaps, for instance, around A. Within these gaps, waves are hindered only when propagating along the specific direction (dictated by the sign of the related wavenumber); conversely, they are fully transmitted when propagating along the opposite direction [29]. This directional wave-filtering is usually accompanied by the generation of lower/higher-order waves at the phase-matched frequencies, thus resulting in a reflection combined with a frequency conversion [19]. Evidence of these effects is provided in the next section where the steady-state solution of waves propagating along a finite modulated metabeam is computed.

3.1.2. Steady-state solutions

To evidence the non-reciprocal behavior predicted by the dispersion analysis, we utilize Eq. (17c) to compute the steady-state response of a finite metabeam. In particular, we are interested in verifying the non-reciprocal reflection/transmission in the directional band gap at pair A in Fig. 3. As an example, an array of 50 resonators is considered for these investigations. The response is recorded at locations x_r and x_t, and later used to compute the reflection and transmission values, respectively. In both scenarios, the harmonic point source $e^{i\omega t}$ and the receiver are located at distances of $d_s = 600a$ and $d_r = 300a$ from the closest oscillator.

According to the formulation discussed in Section 2, the impedance operators $\mathbf{Z}_1$ to $\mathbf{Z}_N$ are obtained from Eq. (13) while the Pth order Green's function in Eq. (20) is obtained by applying the inverse Fourier transform to Eq. (35) as:

$$\hat{G}_w^{(P)}(x, \omega + P\omega_m) = \frac{-1}{4D\beta_P^3}(e^{-\beta_P|x|} + i\, e^{-i\beta_P|x|}), \tag{41}$$

where the Pth order wavenumber for flexural waves reads:

$$\beta_P = \sqrt[4]{\frac{\rho\mathcal{A}(\omega + P\omega_m)^2}{D}}. \tag{42}$$

Substituting Eq. (41) into Eq. (20) we obtain the elastic force coefficients $\hat{\mathbf{F}}_n$, which are inserted into Eq. (17c) for the calculation of the displacement components $\hat{\mathbf{w}}(x)$ in the beam.

We begin our investigation by considering a left-propagating ($\kappa < 0$) flexural wave at frequency $\omega = 1.66\omega_0$, i.e., the intersection at pair A in Fig. 3a. The transmission coefficient, normalized with respect to the incident wave, $|w_t/w_0|$ is displayed in Fig. 3c, considering the scattered waves truncated at $P = \pm 5$ order. As expected, left-propagating incident waves can travel through the resonators almost undisturbed. Conversely, right-propagating ($\kappa > 0$) waves at $\omega = 1.66\omega_0$ undergo a strong reflection with different frequency contents, as shown by the reflection coefficient $|w_r/w_0|$ in Fig. 3d. The largest response occurs at the first-order harmonic ($1.66\omega_0 - \omega_m$), with additional non-negligible components at the second ($1.66\omega_0 - 2\omega_m$) and third-order harmonic ($1.66\omega_0 - 3\omega_m$); the amplitude of other higher-order harmonics is, instead, negligible. To verify the predictions provided by our approach, we compute the same transmission and reflection coefficients using the transfer matrix method. The results, which are marked by solid lines in Figs. 3c,d, are in excellent agreement with our analytical solutions (see more details on the transfer matrix method in Appendix A).

Additionally, we investigate the influence of scatterers number N on the relative strength of the non-reciprocity. To this end, we compute and display the reflection coefficient $|w_r/w_0|$ for right-propagating incident waves at $\omega = 1.66\omega_0$ by considering arrays with an increasing number of oscillators from $N = 1$ to 100, with all other parameters remaining constant. The amplitude of the normalized reflection coefficient for the fundamental ($\omega = 1.66\omega_0$) and first higher-order harmonic ($1.66\omega_0 - \omega_m$) is provided in Fig. 4. The latter markedly increases with the number of scatterers until reaching saturation at approximately $N = 30$, namely a length approximately equal to double the modulation wavelength.

3.2. Modeling non-reciprocal Rayleigh wave propagation in a space–time modulated metasurface

We now consider the propagation of Rayleigh waves across a cluster of modulated resonators. Such a problem has been recently investigated with the aid of FE numerical simulations [20,21]. Our purpose is to show the capability of the proposed analytical formulation to reproduce both the non-reciprocal dispersion and the reflection/transmission coefficients in this complex configuration.

For our example, we consider the parameters recently used in Ref. [21]: a half-space with $c_L/c_T = 2$, a resonator with mass ratio $m_0\omega_0/(\rho a c_T) = 0.15$, the modulation frequency $\omega_m/\omega_0 = 0.25$, and the modulation wavenumber $\kappa_m/\kappa_r = 2.5$, in which $\kappa_r = \omega_0/c_T$.

3.2.1. Dispersion relation

Let us briefly recall the Green's function for a 2D isotropic elastic half-space actuated by a harmonic vertical load acting at the surface. For this configuration, the equilibrium equation can be formulated as a boundary value problem:

$$c_L^2\nabla(\nabla\cdot\mathbf{u}) - c_T^2\nabla\times(\nabla\times\mathbf{u}) = \frac{\partial^2\mathbf{u}}{\partial t^2}, \quad \text{for } z < 0, \tag{43a}$$

$$\tau_{zx}(x,0) = 0, \quad \sigma_z(x,0) = \delta(x)e^{i\omega_P t}, \tag{43b}$$

in which c_L and c_T denote the longitudinal (L) and transverse (T) wave velocities, and τ_{zx}, σ_z represent the shear and normal stresses, respectively; $\mathbf{u}$ is the displacement field with components u and w; $\delta(x)$ is the Dirac delta function.

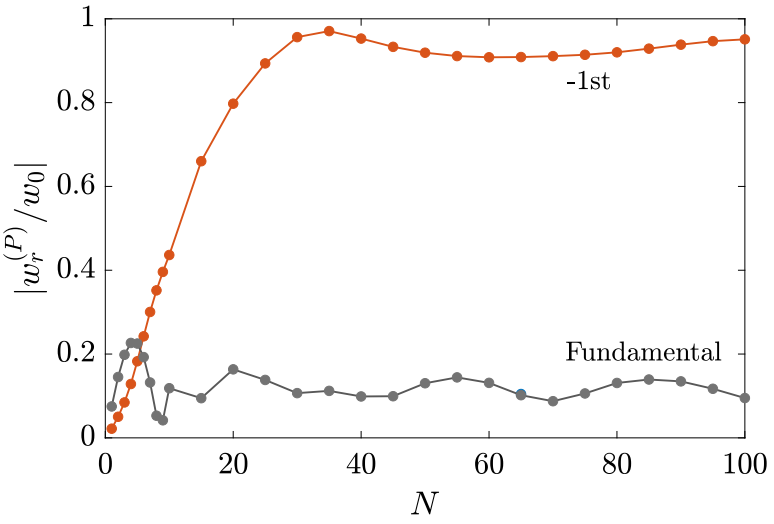

Fig. 4. The influence of scatterers number N on the reflection coefficient $|w_r/w_0|$.

In analogy with the metabeam problem, we Fourier transform the equilibrium Eqs. (43a) and (43b) along the x direction, and obtain the transformed Pth order Green's function at $z = 0$ as:

$$\tilde{G}(\kappa_P, \omega_P) = \frac{1}{\rho c_T^4} \frac{\omega_P^2 \sqrt{\kappa_P^2 - \frac{\omega_P^2}{c_L^2}}}{4\kappa_P^2 \sqrt{\left(\kappa_P^2 - \frac{\omega_P^2}{c_T^2}\right)\left(\kappa_P^2 - \frac{\omega_P^2}{c_L^2}\right)} - \left(2\kappa_P^2 - \frac{\omega_P^2}{c_T^2}\right)^2}, \tag{44}$$

where ρ is the density of the substrate, and the shifted frequency ω_P and wavenumber κ_P are defined in Eq. (36). Substituting Eqs. (37) and (44) into Eq. (31) and setting $P = 0$, we obtain immediately the dispersion relation for Rayleigh waves existing in a non-modulated metasurface:

$$C(\kappa, \omega) := \left(2\kappa^2 - \frac{\omega^2}{c_T^2}\right)^2 - 4\kappa^2 \sqrt{\left(\kappa^2 - \frac{\omega^2}{c_T^2}\right)\left(\kappa^2 - \frac{\omega^2}{c_L^2}\right)} - \frac{m_0 \omega^4 \sqrt{\kappa^2 - \frac{\omega^2}{c_L^2}}}{\rho a c_T^4 (\omega^2/\omega_0^2 - 1)} = 0. \tag{45}$$

This dispersion equation is identical to the one obtained in Refs. [41,42], and matches the numerical dispersion curve computed via FEM, see Appendix B.

As for the metabeam scenario, we first plot the unmodulated $C(\kappa, \omega)$ and the shifted $C(\kappa_P, \omega_P)$ dispersion curves for $P = \pm 1$, Fig. 5a. Again, phase matching points (e.g., pairs A to E) are found when $C(\kappa, \omega) = C(\kappa_P, \omega_P)$ is met. We predict the dispersion properties of the modulated metasurface around these points using Eq. (31). To this purpose, we substitute Eq. (44) into Eq. (31) and truncate the expansion to the first order, using the impedance operator $\mathbf{Z}$ computed according to Eq. (38).

We display the modulated dispersion relation in the range of $\pm 0.1\kappa$ and $\pm 0.1\omega$ around each intersection in Fig. 5b (red circular markers). As an example, the intersection between contra-directional branches gives rise to the locking pair C which results in a directional band gap. Harmonic waves propagating with wavenumber–frequency falling within the directional gap $(1.21\kappa_r, 1.185\omega_0)$ are reflected by the metasurface as a propagating mode at the phase-matched frequency–wavenumber pair $(1.21\kappa_r - \kappa_m, 1.185\omega_0 - \omega_m)$. Conversely, such reflection by conversion does not occur for waves propagating along the opposite direction at the same frequency $1.185\omega_0$, confirming the non-reciprocity due to the broken time-reversal symmetry [21]. Again, clear evidence of these effects predicted by the dispersion curve is provided in the next section by computing the steady-state solutions of Rayleigh waves propagating along a finite modulated metasurface.

3.2.2. Steady-state solutions

To show the non-reciprocal Rayleigh wave propagation discussed above, we use Eq. (17c) to compute the steady-state response of a finite metasurface. The impedance operators $\mathbf{Z}_1$ to $\mathbf{Z}_N$ are computed from Eq. (13), while the Green's function in Eq. (20) is obtained by applying the inverse Fourier transform to Eq. (44), yielding the Pth order wave field (Green's function) at $z = 0$:

$$\hat{G}_w^{(P)}(x, 0, \omega_P) = \frac{1}{2\pi\rho c_T^4} \int_{-\infty}^{\infty} \frac{\omega_P^2 \sqrt{\kappa_P^2 - \frac{\omega_P^2}{c_L^2}}}{4\kappa_P^2 \sqrt{\left(\kappa_P^2 - \frac{\omega_P^2}{c_T^2}\right)\left(\kappa_P^2 - \frac{\omega_P^2}{c_L^2}\right)} - \left(2\kappa_P^2 - \frac{\omega_P^2}{c_T^2}\right)^2} e^{i\kappa_P x} \, d\kappa_P. \tag{46}$$

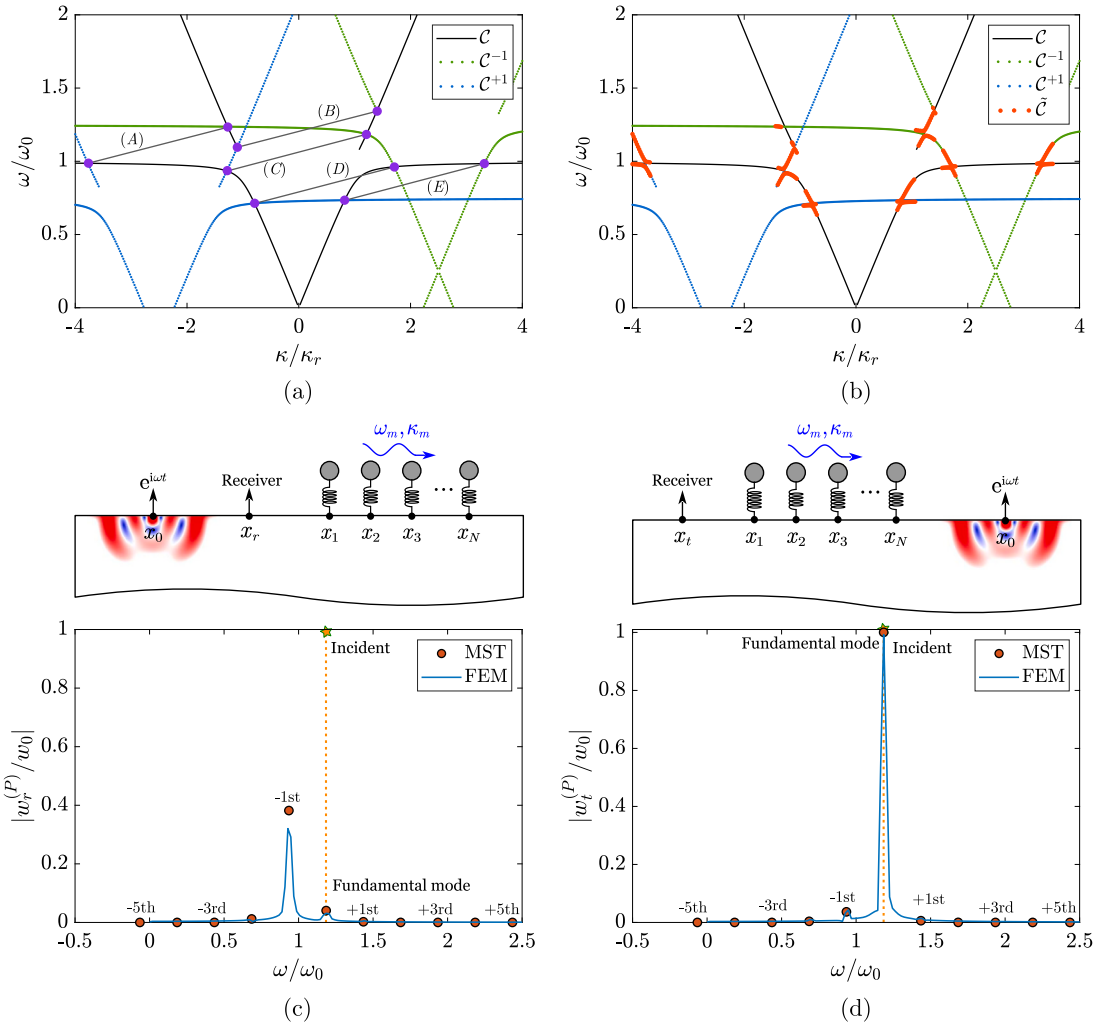

Fig. 5. Analytical modeling of a metasurface. (a) Dispersion relation of a non-modulated metasurface (black solid lines) and its shifted analogs for $P = -1$ and $P = 1$, respectively. (b) Dispersion relation (circular markers) of a modulated metasurface in the vicinity of phase matching pairs. Steady-state solutions of Rayleigh wave propagation at $\omega = 1.185\omega_0$ inside the narrow directional band gap (pair C) for (c) a right and (d) a left traveling incident wave (star marker), respectively.

We note that unlike the Green's function of an Euler beam, Eq. (41), the one for a 2D elastic substrate is divergent at the origin, Eq. (46). To avoid any convergence issue, we introduce a small footprint of length ℓ_s for each resonator so that the associated Green's functions are [39]:

$$\hat{G}_w^{(P)}(x,z,\omega_P) = \frac{1}{\pi\rho c_T^2}\int_{-\infty}^{\infty}\frac{\sin(\kappa_P\ell_s/2)}{\kappa_P}\frac{2\kappa_P^2\beta_L e^{\beta_T z} - \beta_L(2\kappa_P^2 - \frac{\omega_P^2}{c_T^2})e^{\beta_L z}}{4\kappa_P^2\beta_L\beta_T - \left(2\kappa_P^2 - \frac{\omega_P^2}{c_T^2}\right)^2}e^{i\kappa_P x}\,d\kappa_P, \tag{47a}$$

for the vertical displacement components and

$$\hat{G}_u^{(P)}(x,z,\omega_P) = \frac{i}{\pi\rho c_T^2}\int_{-\infty}^{\infty}\sin(\kappa_P\ell_s/2)\frac{2\beta_L\beta_T e^{\beta_T z} - (2\kappa_P^2 - \frac{\omega_P^2}{c_T^2})e^{\beta_L z}}{4\kappa_P^2\beta_L\beta_T - \left(2\kappa_P^2 - \frac{\omega_P^2}{c_T^2}\right)^2}e^{i\kappa_P x}\,d\kappa_P, \tag{47b}$$

for the horizontal ones, where:

$$\beta_L = \sqrt{\kappa_P^2 - \frac{\omega_P^2}{c_L^2}}, \quad \beta_T = \sqrt{\kappa_P^2 - \frac{\omega_P^2}{c_T^2}}. \tag{48}$$

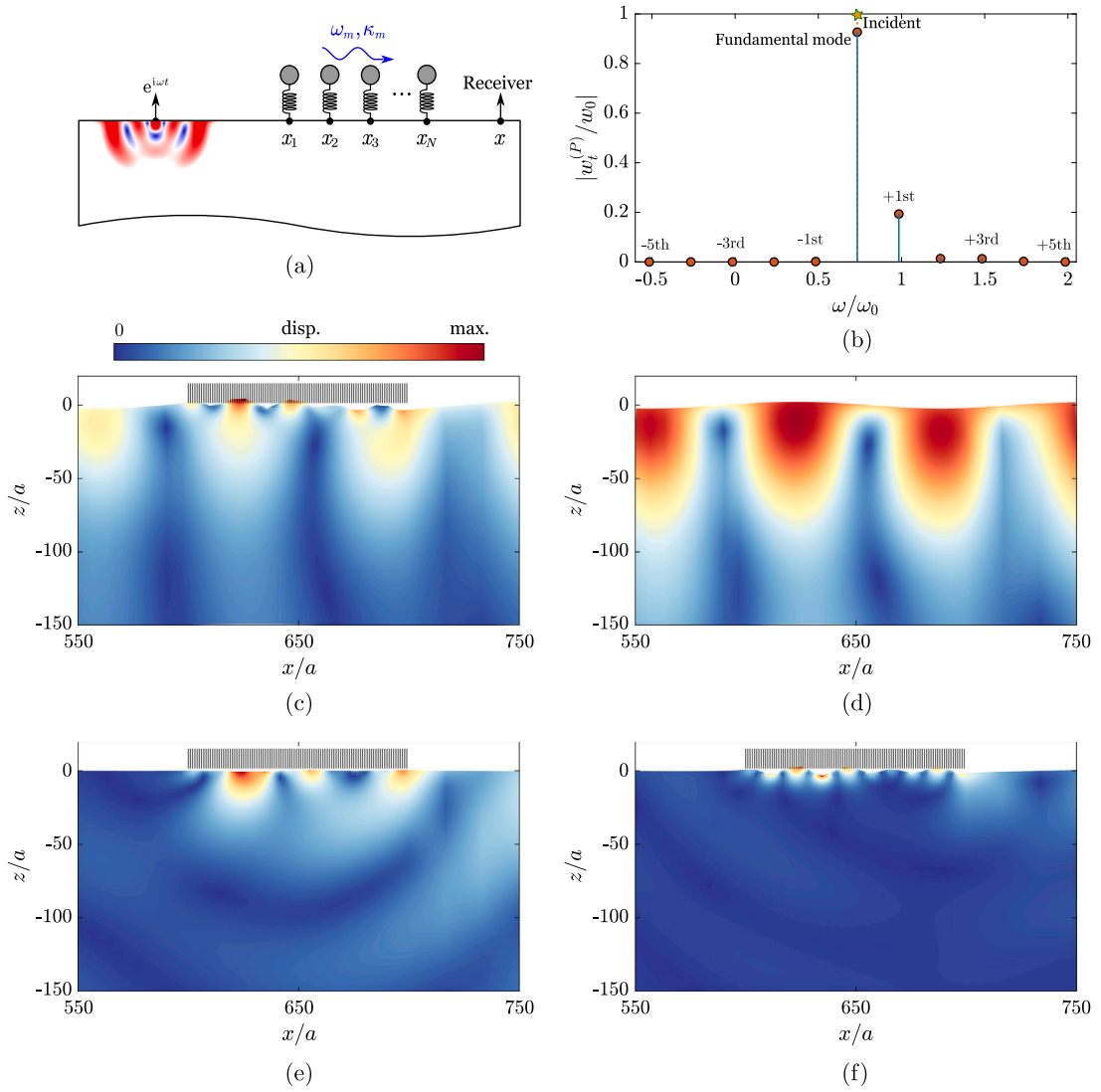

Fig. 6. Harmonic responses of a modulated metasurface. (a) Schematic for right-propagating Rayleigh waves. (b) Steady-state solutions of Rayleigh wave propagation at $\omega = 0.734\omega_0$ (pair E in Fig. 5). The total wave field, free field, fundamental scattered field ($\omega = 0.734\omega_0$), and the first-order scattered field ($\omega = 0.734\omega_0 + \omega_m$) excited by the source at $\omega = 0.734\omega_0$ are shown in (c), (d), (e) and (f), respectively.

Substituting Eq. (47a) into Eq. (20) we obtain the elastic force coefficients $\hat{\mathbf{F}}_n$, which are used in Eqs. (17a), (17c) to compute the wave field $\hat{\mathbf{u}}(x,z)$, $\hat{\mathbf{w}}(x,z)$ in the substrate.

For our example, we compute the steady-state response at locations $(x_r,0)$ and $(x_t,0)$ on the substrate surface considering an array of 100 resonators with footprint width $\ell_s = a/20$, where the harmonic point source and the receiver are located at distances of $d_s = 600a$ and $d_r = 300a$ from the closest resonator. For a right-going ($\kappa > 0$) incident Rayleigh wave (dashed line) at $\omega = 1.185\omega_0$ the reflected field, shown in Fig. 5c, confirms a back-scattering at the coupled frequency $\omega = 1.185\omega_0 - \omega_m$. Conversely, the left-going ($\kappa < 0$) incident Rayleigh wave (dashed line) at the same frequency $\omega = 1.185\omega_0$ propagates without reflection or frequency conversion phenomena (see Fig. 5d).

We now resort to the FEM to verify our analytical solutions. To this purpose, we build a 2D plane-strain model in commercial FE software (COMSOL Multiphysics). The reader can find the details of the numerical model in Appendix C. Specifically, we compute the transient response of the system actuated by a vertical tone-burst-shaped force having central frequency $\omega = 1.185\omega_0$, and analyze the vertical displacement field w (see the insets of Fig. 5). The corresponding frequency spectra (solid line) computed through the Fourier transform (FFT) of the record time-domain data at the receiver are displayed in Figs. 5c,d. The reader can appreciate how the numerical results match the analytical solutions.

Finally, we inspect the steady-state response at the "veering pair" (intersection between two co-directional branches) [21] E in Fig. 5, where we expect the Rayleigh wave to be transmitted and converted from one harmonic to another [20,21]. To evidence

such a conversion, we utilize the same model (see Fig. 6) excited by a right-going incident Rayleigh wave at frequency $\omega = 0.734\omega_0$. The results obtained with both the analytical solutions and the FE model are collected in Fig. 6b. The modulated metasurface can convert the incident wave ($\omega = 0.734\omega_0$) into a transmitted wave with a different frequency content, e.g., the phase matched first-order harmonic at $\omega = 0.734\omega_0 + \omega_m$.

To better appreciate this effect, we compute the total wave field $\sqrt{\Re(u)^2 + \Re(w)^2}$, using Eqs. (17a), (17c), (47a), (47b), in the domain $x = [550, 750]a$, $z = [-150, 0]a$. The total wave field, shown in Fig. 6c, can be decomposed by Eqs. (17a), (17c) into the incident field at $\omega = 0.734\omega_0$, Fig. 6d, and scattered wave fields: the fundamental mode at $\omega = 0.734\omega_0$ in Fig. 6e and the first-order harmonic at $\omega = 0.734\omega_0 + \omega_m$ in Fig. 6f. Both scattering fields exhibit a clear asymmetry, with the right-hand side having a greater amplitude than the left-hand side, a clear feature of the forward scattering behavior at veering pairs of the modulated metasurface.

4. Conclusion

We developed a multiple scattering formulation to model the interaction of a given incident field with a cluster of space–time-modulated resonators located at the surface of a given elastic waveguide. The effect of time-varying resonators is modeled by means of impedance operators, able to account for lower- and higher-order harmonics generated by the modulated oscillators. The vertical motion of resonators, actuated by the incident field, generates scattered fields in the waveguide, which are characterized via ad-hoc Green's functions. The unknown amplitudes of scattered fields are then obtained from a multiple scattering scheme by ensuring the continuity of displacement at the footprint of resonators.

We have demonstrated the capabilities and accuracy of our framework by computing both the dispersion relation and wave field of flexural and Rayleigh waves propagating along modulated beams and substrates, respectively.

Our approach has several advantages compared to currently available methods for studying elastic waves along space–time-modulated metamaterials. First, it allows to investigate an arbitrary number of resonators with no restriction on their spatial configuration and modulation profile, apart from their common modulation period T_m. Second, it enables the analytical treatment of non-reciprocal wave propagation in higher dimensional systems (2D and 3D), thus overcoming the limitation of currently available analytical methods (e.g., the transfer matrix method) valid only for 1D wave propagation problems [31]. Third, our method is able to reduce the computational cost with respect to classical numerical schemes since it does not require the discretization of the entire system. This feature is particularly appealing for modeling wave propagation in higher dimensional systems and will prove its value for future design and optimization studies. Fourth, it advances the knowledge of multiple scattering theory which has demonstrated its superior capabilities in modeling the interaction of oscillators with elastic flexural and surface acoustic waves [37–39,43,44].

As such, the proposed formulation can serve as a valuable tool to explore various modulation profiles on elastic waveguides and to guide future experiments on space–time-modulated systems. Since the framework developed in this work is general, we also expect an extension into acoustics and electromagnetism, thus supporting the development of nonreciprocal devices for both acoustics and optics.

CRediT authorship contribution statement

Xingbo Pu: Conceptualization, Data curation, Formal analysis, Investigation, Methodology, Software, Writing – original draft. **Alessandro Marzani:** Conceptualization, Formal analysis, Funding acquisition, Supervision, Validation, Writing – review & editing. **Antonio Palermo:** Conceptualization, Formal analysis, Investigation, Methodology, Supervision, Validation, Writing – review & editing.

Declaration of competing interest

The authors declare that they have no known competing financial interests or personal relationships that could have appeared to influence the work reported in this paper.

Data availability

Data will be made available on request.

Acknowledgments

This project has received funding from the European Union's Horizon 2020 research and innovation programme under the Marie Skłodowska Curie grant agreement No 813424.

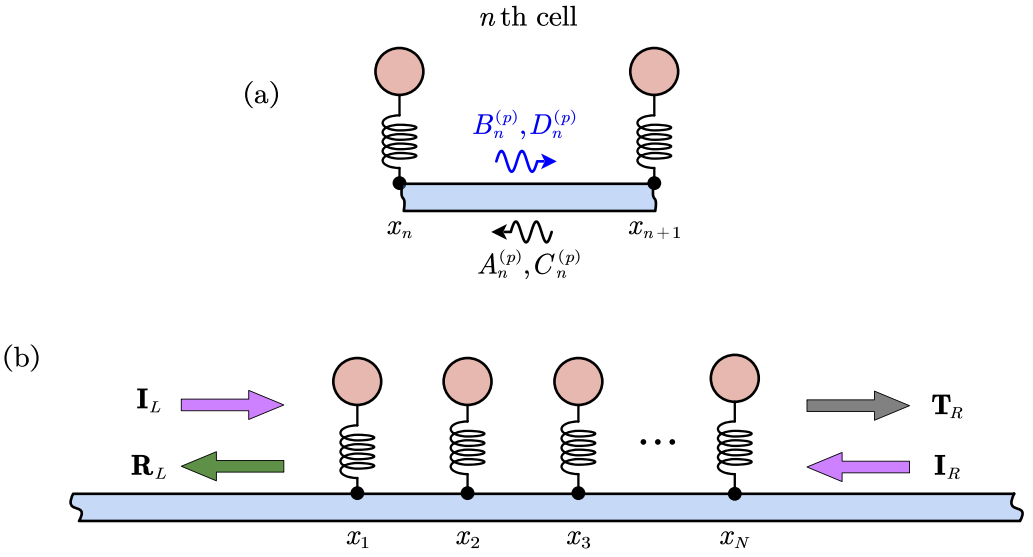

Fig. A.1. Schematic of transfer matrix method: (a) the nth cell, (b) the global system.

Appendix A. Details on the transfer matrix method (TMM)

In this Appendix, we provide the details of the transfer matrix method for the modulated beam (see Fig. A.1) [22]. According to Euler beam theory, the pth order displacement in the nth cell can be expressed as:

$$\hat{w}_n^{(p)}(x) = [\mathrm{e}^{\mathrm{i}\beta^{(p)}(x-x_n)}, \mathrm{e}^{-\mathrm{i}\beta^{(p)}(x-x_n)}, \mathrm{e}^{\beta^{(p)}(x-x_n)}, \mathrm{e}^{-\beta^{(p)}(x-x_n)}][A_n^{(p)}, B_n^{(p)}, C_n^{(p)}, D_n^{(p)}]^T := \mathcal{L}_n^{(p)}(x)\mathbf{U}_n^{(p)}, \tag{A.1}$$

in which $\beta^{(p)} = \sqrt[4]{\rho\mathcal{A}(\omega + p\omega_m)^2/\mathcal{D}}$ is the pth order wavenumber.

By truncating the orders from $p = -P$ to $p = P$, the displacement can be expressed in matrix form $\hat{\mathbf{w}}_n(x) = \mathbf{L}_n(x)\mathbf{A}_n$, with:

$$\hat{\mathbf{w}}_n(x) = \begin{bmatrix} \hat{w}^{(-P)}(x) \\ \hat{w}^{(-P+1)}(x) \\ \vdots \\ \hat{w}^{(P)}(x) \end{bmatrix}, \ \mathbf{L}_n(x) = \begin{bmatrix} \mathcal{L}_n^{(-P)}(x) & \mathbf{0} & \cdots & \mathbf{0} \\ \mathbf{0} & \mathcal{L}_n^{(-P+1)}(x) & \cdots & \mathbf{0} \\ \vdots & \vdots & \ddots & \vdots \\ \mathbf{0} & \mathbf{0} & \cdots & \mathcal{L}_n^{(P)}(x) \end{bmatrix}, \ \mathbf{A}_n = \begin{bmatrix} \mathbf{U}_n^{(-P)} \\ \mathbf{U}_n^{(-P+1)} \\ \vdots \\ \mathbf{U}_n^{(P)} \end{bmatrix}. \tag{A.2}$$

Hence, the vertical force $\hat{\mathbf{F}}_n$ in Eq. (13) can be written as:

$$\hat{\mathbf{F}}_n = \mathbf{D}_n\mathbf{M}_n^{-1}\mathbf{Q}_n\hat{\mathbf{w}}_n(x_n) = \mathbf{D}_n\mathbf{M}_n^{-1}\mathbf{Q}_n\mathbf{L}_n(x_n)\mathbf{A}_n. \tag{A.3}$$

For an arbitrary pth order, the continuities of the displacement, slope, bending moment and shear force at x_n yield:

$$\hat{w}_{n-1}^{(p)}(x_n) = \hat{w}_n^{(p)}(x_n), \tag{A.4a}$$

$$\frac{\partial}{\partial x}\hat{w}_{n-1}^{(p)}(x_n) = \frac{\partial}{\partial x}\hat{w}_n^{(p)}(x_n), \tag{A.4b}$$

$$\mathcal{D}\frac{\partial^2}{\partial x^2}\hat{w}_{n-1}^{(p)}(x_n) = \mathcal{D}\frac{\partial^2}{\partial x^2}\hat{w}_n^{(p)}(x_n), \tag{A.4c}$$

$$\mathcal{D}\frac{\partial^3}{\partial x^3}\hat{w}_{n-1}^{(p)}(x_n) = \mathcal{D}\frac{\partial^3}{\partial x^3}\hat{w}_n^{(p)}(x_n) - \hat{F}_n^{(p)}. \tag{A.4d}$$

Substituting Eq. (A.1) into Eqs. (A.4a)–(A.4d) yields:

$$\boldsymbol{\alpha}_{n-1}^{(p)}\mathbf{U}_{n-1}^{(p)} = \boldsymbol{\zeta}_n^{(p)}\mathbf{U}_n^{(p)} + \boldsymbol{\gamma}_n^{(p)}, \tag{A.5}$$

with the coefficients:

$$\boldsymbol{\alpha}_{n-1}^{(p)} = \begin{bmatrix} \mathrm{e}^{\mathrm{i}\beta^{(p)}\ell_n} & \mathrm{e}^{-\mathrm{i}\beta^{(p)}\ell_n} & \mathrm{e}^{\beta^{(p)}\ell_n} & \mathrm{e}^{-\beta^{(p)}\ell_n} \\ \mathrm{i}\mathrm{e}^{\mathrm{i}\beta^{(p)}\ell_n} & -\mathrm{i}\mathrm{e}^{-\mathrm{i}\beta^{(p)}\ell_n} & \mathrm{e}^{\beta^{(p)}\ell_n} & -\mathrm{e}^{-\beta^{(p)}\ell_n} \\ -\mathrm{e}^{\mathrm{i}\beta^{(p)}\ell_n} & -\mathrm{e}^{-\mathrm{i}\beta^{(p)}\ell_n} & \mathrm{e}^{\beta^{(p)}\ell_n} & \mathrm{e}^{-\beta^{(p)}\ell_n} \\ -\mathrm{i}\mathrm{e}^{\mathrm{i}\beta^{(p)}\ell_n} & \mathrm{i}\mathrm{e}^{-\mathrm{i}\beta^{(p)}\ell_n} & \mathrm{e}^{\beta^{(p)}\ell_n} & -\mathrm{e}^{-\beta^{(p)}\ell_n} \end{bmatrix}, \ \boldsymbol{\zeta}_n^{(p)} = \begin{bmatrix} 1 & 1 & 1 & 1 \\ \mathrm{i} & -\mathrm{i} & 1 & -1 \\ -1 & -1 & 1 & 1 \\ -\mathrm{i} & \mathrm{i} & 1 & -1 \end{bmatrix}, \ \boldsymbol{\gamma}_n^{(p)} = \begin{bmatrix} 0 \\ 0 \\ 0 \\ \hat{F}_n^{(p)}\chi^{(p)} \end{bmatrix}, \tag{A.6}$$

where $\ell_n = x_n - x_{n-1}$, and $\chi^{(p)} = -1/[(\beta^{(p)})^3 D]$. Similarly, by truncating the orders from $-P$ to P, the displacements can be expressed in matrix form:

$$\boldsymbol{\alpha}\mathbf{A}_{n-1} = \boldsymbol{\zeta}\mathbf{A}_n + \boldsymbol{\gamma}\hat{\mathbf{F}}_n, \tag{A.7}$$

with:

$$\boldsymbol{\alpha} = \begin{bmatrix} \boldsymbol{\alpha}_{n-1}^{(-P)} & & & \\ & \boldsymbol{\alpha}_{n-1}^{(-P+1)} & & \\ & & \ddots & \\ & & & \boldsymbol{\alpha}_{n-1}^{(P)} \end{bmatrix}, \ \boldsymbol{\zeta} = \begin{bmatrix} \boldsymbol{\zeta}_n^{(-P)} & & & \\ & \boldsymbol{\zeta}_n^{(-P+1)} & & \\ & & \ddots & \\ & & & \boldsymbol{\zeta}_n^{(P)} \end{bmatrix}, \ \boldsymbol{\gamma} = \begin{bmatrix} 0 & 0 & \cdots & 0 \\ 0 & 0 & \cdots & 0 \\ 0 & 0 & \cdots & 0 \\ \chi^{(-P)} & 0 & \cdots & 0 \\ 0 & 0 & \cdots & 0 \\ 0 & 0 & \cdots & 0 \\ 0 & 0 & \cdots & 0 \\ 0 & \chi^{(-P+1)} & \cdots & 0 \\ \vdots & \vdots & \ddots & \vdots \\ 0 & 0 & \cdots & 0 \\ 0 & 0 & \cdots & 0 \\ 0 & 0 & \cdots & 0 \\ 0 & 0 & \cdots & \chi^{(P)} \end{bmatrix} \tag{A.8}$$

Combining Eqs. (A.3) and (A.7) we obtain:

$$\boldsymbol{\alpha}\mathbf{A}_{n-1} = \boldsymbol{\zeta}\mathbf{A}_n + \boldsymbol{\gamma}\mathbf{D}_n\mathbf{M}_n^{-1}\mathbf{Q}_n\mathbf{L}_n(x_n)\mathbf{A}_n, \tag{A.9}$$

from which we obtain the local transfer matrix relating $\mathbf{A}_{n-1}$ to $\mathbf{A}_n$:

$$\mathbf{T}_n\mathbf{A}_{n-1} = \mathbf{A}_n, \tag{A.10}$$

where:

$$\mathbf{T}_n = [\boldsymbol{\zeta} + \boldsymbol{\gamma}\mathbf{D}_n\mathbf{M}_n^{-1}\mathbf{Q}_n\mathbf{L}_n(x_n)]^{-1}\boldsymbol{\alpha}. \tag{A.11}$$

Therefore, for an infinite beam coupled with N resonators, the global equation is expressed as:

$$\mathcal{T}\mathbf{A}_0 = \mathbf{A}_N, \tag{A.12}$$

where the global transfer matrix $\mathcal{T}$ reads:

$$\mathcal{T} = \mathbf{T}_N\mathbf{T}_{N-1}\cdots\mathbf{T}_1. \tag{A.13}$$

After some algebraic operations, Eq. (A.12) can be further written as:

$$\begin{bmatrix} \mathcal{M}_{11} & \mathcal{M}_{12} \\ \mathcal{M}_{21} & \mathcal{M}_{22} \end{bmatrix} \begin{bmatrix} \mathbf{I}_L \\ \mathbf{R}_L \end{bmatrix} = \begin{bmatrix} \mathbf{T}_R \\ \mathbf{I}_R \end{bmatrix}, \tag{A.14}$$

with coefficients:

$$\mathcal{M} = \mathcal{P}\mathcal{T}\mathcal{P}^T, \tag{A.15a}$$

$$\mathbf{I}_L = [B_0^{(-P)}, D_0^{(-P)}, B_0^{(-P+1)}, D_0^{(-P+1)}, \ldots, B_0^{(P)}, D_0^{(P)}]^T, \tag{A.15b}$$

$$\mathbf{R}_L = [A_0^{(-P)}, C_0^{(-P)}, A_0^{(-P+1)}, C_0^{(-P+1)}, \ldots, A_0^{(P)}, C_0^{(P)}]^T, \tag{A.15c}$$

$$\mathbf{T}_R = [B_N^{(-P)}, D_N^{(-P)}, B_N^{(-P+1)}, D_N^{(-P+1)}, \ldots, B_N^{(P)}, D_N^{(P)}]^T, \tag{A.15d}$$

$$\mathbf{I}_R = [A_N^{(-P)}, C_N^{(-P)}, A_N^{(-P+1)}, C_N^{(-P+1)}, \ldots, A_N^{(P)}, C_N^{(P)}]^T, \tag{A.15e}$$

in which $\mathcal{P}$ is an elementary matrix which reads:

$$\mathcal{P} = \begin{bmatrix} 0 & 1 & 0 & 0 & 0 & 0 & \cdots & 0 & 0 \\ 0 & 0 & 0 & 1 & 0 & 0 & \cdots & 0 & 0 \\ 0 & 0 & 0 & 0 & 0 & 1 & \cdots & 0 & 0 \\ \vdots & \vdots & \vdots & \vdots & \vdots & \vdots & \ddots & \vdots & \vdots \\ 0 & 0 & 0 & 0 & 0 & 0 & \cdots & 0 & 1 \\ 1 & 0 & 0 & 0 & 0 & 0 & \cdots & 0 & 0 \\ 0 & 0 & 1 & 0 & 0 & 0 & \cdots & 0 & 0 \\ 0 & 0 & 0 & 0 & 1 & 0 & \cdots & 0 & 0 \\ \vdots & \vdots & \vdots & \vdots & \vdots & \vdots & \ddots & \vdots & \vdots \\ 0 & 0 & 0 & 0 & 0 & 0 & \cdots & 1 & 0 \end{bmatrix}. \tag{A.16}$$

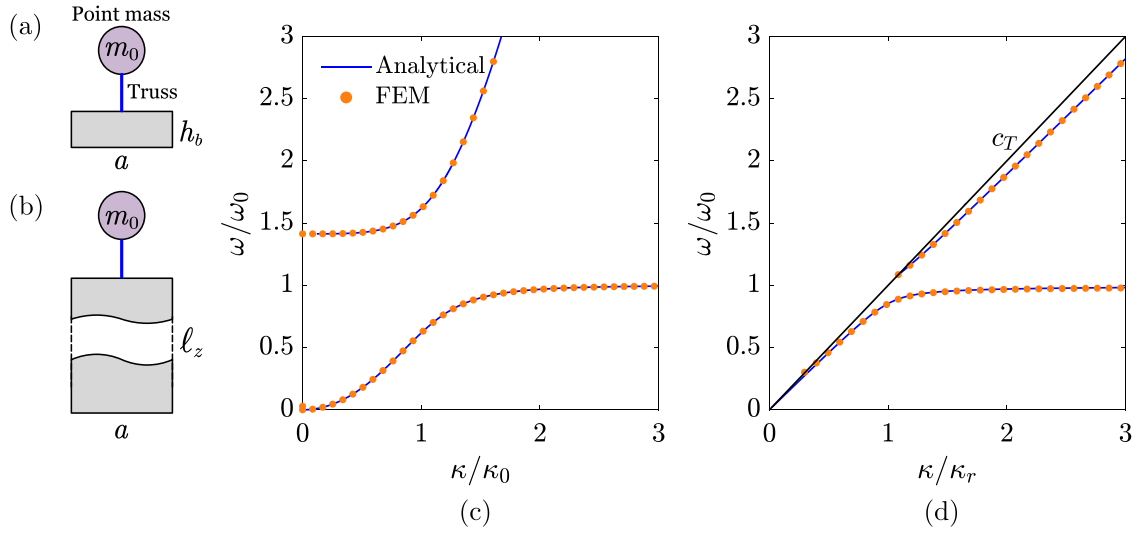

Fig. B.1. Comparison of non-modulated (original) dispersion curves between the analytical solution and the FE solution. (a, b) Schematic of unit cells used for the FE simulation. The dispersion curves for (c) flexural waves in a metabeam, and (d) Rayleigh waves in a metasurface.

Eq. (A.14) can be further transformed to:

$$\boldsymbol{\psi}_{\text{out}} = \mathcal{S}\boldsymbol{\psi}_{\text{in}}, \tag{A.17}$$

where:

$$\boldsymbol{\psi}_{\text{out}} = \begin{pmatrix} \mathbf{R}_L \\ \mathbf{T}_R \end{pmatrix}, \quad \boldsymbol{\psi}_{\text{in}} = \begin{pmatrix} \mathbf{I}_L \\ \mathbf{I}_R \end{pmatrix}, \quad \mathcal{S} = \begin{pmatrix} -\mathcal{M}_{22}^{-1}\mathcal{M}_{21} & \mathcal{M}_{22}^{-1} \\ \mathcal{M}_{11} - \mathcal{M}_{12}\mathcal{M}_{22}^{-1}\mathcal{M}_{21} & \mathcal{M}_{12}\mathcal{M}_{22}^{-1} \end{pmatrix}. \tag{A.18}$$

With Eq. (A.17) we can compute both the transmission and reflection coefficients directly. It is worth mentioning that, due to the presence of exponential amplification terms in $\boldsymbol{\alpha}_{n-1}^{(p)}$ in Eq. (A.5), the transfer matrix method may encounter numerical divergence in some occasions, e.g., when considering a large number of oscillators or large values of resonators spacing. Such a limitation can be well addressed by the multiple scattering formulation proposed in this work.

Appendix B. Validation of non-modulated dispersion equation

In this Appendix, we validate the analytical dispersion equation of non-modulated metamaterials via the finite element method (FEM). To do so, we build 2D FE models (unit cells) using 2D elasticity in COMSOL Multiphysics. In particular, the Euler beam is modeled by a 2D plane-stress FE model with dimensions $a \times h_b$ (Fig. B.1a), while the half-space is modeled by a 2D plane-strain FE model with the height $\ell_z = 4\pi c_T/\omega_0$ (Fig. B.1b). To model the linear spring, we use a truss model with the unit cross-sectional area and unit height whose equivalent Young modulus satisfies $E_t = m_0\omega_0^2$. Additionally, the resonator mass is modeled by a point mass model with mass m_0. To simulate the dynamics of an infinite array of periodic resonators, we impose a pair of Floquet periodic boundary conditions on the vertical substrate edges. In Fig. B.1b, a clamped boundary condition is enforced at the bottom edge to avoid rigid motions.

For the metabeam, the parameters used in this work are set as: mass density $\rho = 2700$ kg/m^3, Young modulus $E = 69$ GPa, Poisson ratio $\nu = 0.33$, lattice constant $a = 0.04$ m, beam thickness $h_b = 0.002$ m, beam width $b_w = 0.03$ m, the resonance frequency of oscillators $\omega_0 = 80\pi$ rad/s, and damping coefficient of oscillators $c = 0$. For the metasurface, the parameters used are: mass density $\rho = 2700$ kg/m^3, Young modulus $E = 69$ GPa, Poisson ratio $\nu = 0.33$, lattice constant $a = 0.3$ m, resonance frequency of oscillators $\omega_0 = 200\pi$ rad/s, and damping coefficient of oscillators $c = 0$. The numerical dispersion curves are obtained by solving the eigenvalue problem for a given wave number varying between $k = [0, \pi/a]$. The comparison between the analytical dispersion curves computed by Eqs. (38), (45) and FE simulations for non-modulated metabeam and metasurface is shown in Fig. B.1c and B.1d, respectively. Excellent agreement between them is observed.

Appendix C. Details on the FE model for transient simulations

In this Appendix, we provide the details of the 2D plane-strain FE model, implemented in COMSOL Multiphysics, used to verify our analytical solutions in Section 3.2.2. The FE model consists of an array of resonators and a substrate with width $\ell_x = 32\lambda_0$ and depth $\ell_x = 8\lambda_0$, where $\lambda_0 = 2\pi c_T/\omega_0$ (see Figs. C.1a,b). As in Appendix B, the resonator is modeled by a point mass m_0, while the spring is modeled by a truss element with unit length and cross-sectional area whose Young modulus reads $E_t = k_0 + k_a \cos(\omega_m t - \kappa_m x)$.

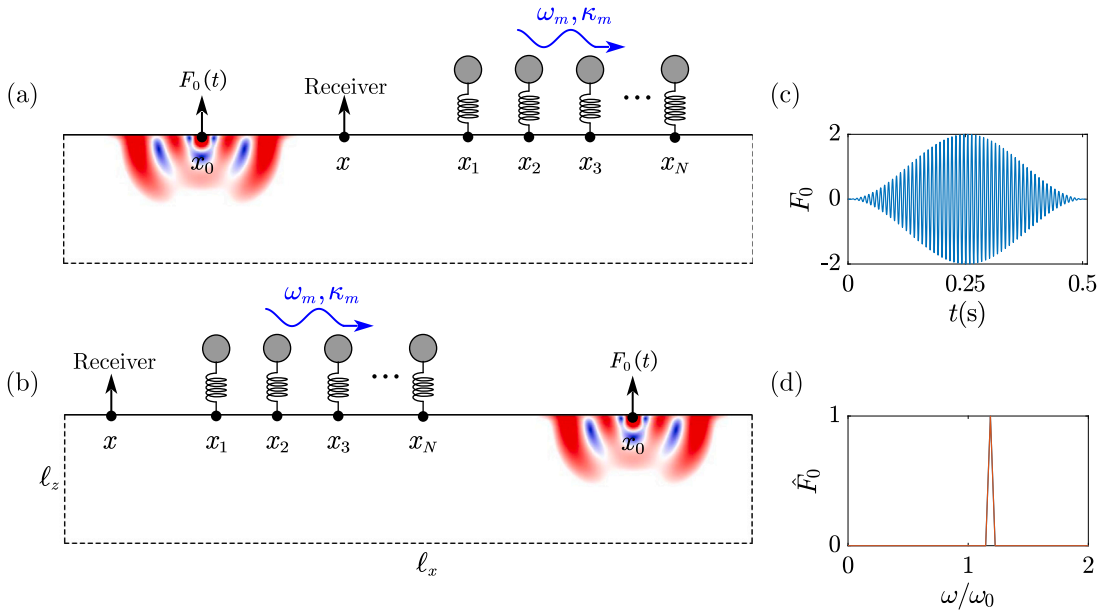

Fig. C.1. Schematic of the FE model for transient simulations.

To minimize reflections from the domain borders, we add low-reflecting boundary conditions around the substrate (denoted by the dashed lines). The substrate is discretized using a fine mesh ($\lambda_0/10$) of quadratic serendipity elements, which allows us to obtain convergent results at the frequency of interest.

We perform numerical simulations in the time domain. A narrow tone-burst signal of the form $F_0(t) = A_0[H(t) - H(t - 2\pi N/\omega)]\sin(\omega t)[1-\cos(\omega t/N)]$ is used to generate Rayleigh waves, where $H(t)$ is the Heaviside function. In the numerical example, the amplitude is set as $A_0 = 1$, the central frequency is $\omega = 1.185\omega_0$, and the number of cycles is $N = 60$. We display the signal and its Fourier spectrum in Figs. C.1c,d.

References

[1] H. Nassar, B. Yousefzadeh, R. Fleury, M. Ruzzene, A. Alù, C. Daraio, A.N. Norris, G. Huang, M.R. Haberman, Nonreciprocity in acoustic and elastic materials, Nat. Rev. Mater. 5 (9) (2020) 667–685, http://dx.doi.org/10.1038/s41578-020-0206-0.

[2] Y. Chen, X. Li, C. Scheibner, V. Vitelli, G. Huang, Realization of active metamaterials with odd micropolar elasticity, Nature Commun. 12 (1) (2021) 1–12, http://dx.doi.org/10.1038/s41467-021-26034-z.

[3] D.L. Sounas, A. Alu, Non-reciprocal photonics based on time modulation, Nat. Photonics 11 (12) (2017) 774–783, http://dx.doi.org/10.1038/s41566-017-0051-x.

[4] R. Fleury, D.L. Sounas, A. Alù, Subwavelength ultrasonic circulator based on spatiotemporal modulation, Phys. Rev. B 91 (17) (2015) 174306, http://dx.doi.org/10.1103/PhysRevB.91.174306.

[5] C. Rasmussen, L. Quan, A. Alù, Acoustic nonreciprocity, J. Appl. Phys. 129 (21) (2021) 210903, http://dx.doi.org/10.1063/5.0050775.

[6] B.M. Goldsberry, S.P. Wallen, M.R. Haberman, Non-reciprocal wave propagation in mechanically-modulated continuous elastic metamaterials, J. Acoust. Soc. Am. 146 (1) (2019) 782–788, http://dx.doi.org/10.1121/1.5115019.

[7] X. Xu, Q. Wu, H. Chen, H. Nassar, Y. Chen, A. Norris, M.R. Haberman, G. Huang, Physical observation of a robust acoustic pumping in waveguides with dynamic boundary, Phys. Rev. Lett. 125 (25) (2020) 253901, http://dx.doi.org/10.1103/PhysRevLett.125.253901.

[8] E. Riva, G. Castaldini, F. Braghin, Adiabatic edge-to-edge transformations in time-modulated elastic lattices and non-Hermitian shortcuts, New J. Phys. 23 (9) (2021) 093008, http://dx.doi.org/10.1088/1367-2630/ac1ed4.

[9] Q. Wu, X. Zhang, P. Shivashankar, Y. Chen, G. Huang, Independent flexural wave frequency conversion by a linear active metalayer, Phys. Rev. Lett. 128 (24) (2022) 244301, http://dx.doi.org/10.1103/PhysRevLett.128.244301.

[10] B. Liang, X. Guo, J. Tu, D. Zhang, J. Cheng, An acoustic rectifier, Nature Mater. 9 (12) (2010) 989–992, http://dx.doi.org/10.1038/nmat2881.

[11] R. Fleury, D.L. Sounas, C.F. Sieck, M.R. Haberman, A. Alù, Sound isolation and giant linear nonreciprocity in a compact acoustic circulator, Science 343 (6170) (2014) 516–519, http://dx.doi.org/10.1126/science.1246957.

[12] R. Fleury, A.B. Khanikaev, A. Alu, Floquet topological insulators for sound, Nature Commun. 7 (1) (2016) 1–11, http://dx.doi.org/10.1038/ncomms11744.

[13] N. Reiskarimian, H. Krishnaswamy, Magnetic-free non-reciprocity based on staggered commutation, Nature Commun. 7 (1) (2016) 1–10, http://dx.doi.org/10.1038/ncomms11217.

[14] M. Jalšić, N. Alujević, T. Garma, I. Ćatipović, M. Jokić, H. Wolf, An active metamaterial cell concept for nonreciprocal vibroacoustic transmission, Mech. Syst. Signal Process. 186 (2023) 109829, http://dx.doi.org/10.1016/j.ymssp.2022.109829.

[15] X. Huang, B. Yang, Towards novel energy shunt inspired vibration suppression techniques: Principles, designs and applications, Mech. Syst. Signal Process. 182 (2023) 109496, http://dx.doi.org/10.1016/j.ymssp.2022.109496.

[16] G. Trainiti, M. Ruzzene, Non-reciprocal elastic wave propagation in spatiotemporal periodic structures, New J. Phys. 18 (8) (2016) 083047, http://dx.doi.org/10.1088/1367-2630/18/8/083047.

[17] H. Nassar, X. Xu, A. Norris, G. Huang, Modulated phononic crystals: Non-reciprocal wave propagation and Willis materials, J. Mech. Phys. Solids 101 (2017) 10–29, http://dx.doi.org/10.1016/j.jmps.2017.01.010.

[18] B.M. Goldsberry, S.P. Wallen, M.R. Haberman, Nonreciprocal vibrations of finite elastic structures with spatiotemporally modulated material properties, Phys. Rev. B 102 (1) (2020) 014312, http://dx.doi.org/10.1103/PhysRevB.102.014312.
[19] H. Nassar, H. Chen, A. Norris, G. Huang, Non-reciprocal flexural wave propagation in a modulated metabeam, Extreme Mech. Lett. 15 (2017) 97–102, http://dx.doi.org/10.1016/j.eml.2017.07.001.
[20] Q. Wu, H. Chen, H. Nassar, G. Huang, Non-reciprocal Rayleigh wave propagation in space–time modulated surface, J. Mech. Phys. Solids 146 (2021) 104196, http://dx.doi.org/10.1016/j.jmps.2020.104196.
[21] A. Palermo, P. Celli, B. Yousefzadeh, C. Daraio, A. Marzani, Surface wave non-reciprocity via time-modulated metamaterials, J. Mech. Phys. Solids 145 (2020) 104181, http://dx.doi.org/10.1016/j.jmps.2020.104181.
[22] Y. Chen, X. Li, H. Nassar, A.N. Norris, C. Daraio, G. Huang, Nonreciprocal wave propagation in a continuum-based metamaterial with space-time modulated resonators, Phys. Rev. A 11 (6) (2019) 064052, http://dx.doi.org/10.1103/PhysRevApplied.11.064052.
[23] G. Trainiti, Y. Xia, J. Marconi, G. Cazzulani, A. Erturk, M. Ruzzene, Time-periodic stiffness modulation in elastic metamaterials for selective wave filtering: Theory and experiment, Phys. Rev. Lett. 122 (12) (2019) 124301, http://dx.doi.org/10.1103/PhysRevLett.122.124301.
[24] J. Marconi, E. Riva, M. Di Ronco, G. Cazzulani, F. Braghin, M. Ruzzene, Experimental observation of nonreciprocal band gaps in a space-time-modulated beam using a shunted piezoelectric array, Phys. Rev. A 13 (3) (2020) 031001, http://dx.doi.org/10.1103/PhysRevApplied.13.031001.
[25] S. Wan, L. Cao, Y. Zeng, T. Guo, M. Oudich, B. Assouar, Low-frequency nonreciprocal flexural wave propagation via compact cascaded time-modulated resonators, Appl. Phys. Lett. 120 (23) (2022) 231701, http://dx.doi.org/10.1063/5.0097501.
[26] M. Attarzadeh, M. Nouh, Non-reciprocal elastic wave propagation in 2D phononic membranes with spatiotemporally varying material properties, J. Sound Vib. 422 (2018) 264–277, http://dx.doi.org/10.1016/j.jsv.2018.02.028.
[27] Z. Chen, Y. Peng, H. Li, J. Liu, Y. Ding, B. Liang, X.-F. Zhu, Y. Lu, J. Cheng, A. Alù, Efficient nonreciprocal mode transitions in spatiotemporally modulated acoustic metamaterials, Sci. Adv. 7 (45) (2021) eabj1198, http://dx.doi.org/10.1126/sciadv.abj1198.
[28] J. Vila, R.K. Pal, M. Ruzzene, G. Trainiti, A bloch-based procedure for dispersion analysis of lattices with periodic time-varying properties, J. Sound Vib. 406 (2017) 363–377, http://dx.doi.org/10.1016/j.jsv.2017.06.011.
[29] H. Nassar, H. Chen, A. Norris, M. Haberman, G. Huang, Non-reciprocal wave propagation in modulated elastic metamaterials, Proc. R. Soc. A 473 (2202) (2017) 20170188, http://dx.doi.org/10.1098/rspa.2017.0188.
[30] Y. Wang, B. Yousefzadeh, H. Chen, H. Nassar, G. Huang, C. Daraio, Observation of nonreciprocal wave propagation in a dynamic phononic lattice, Phys. Rev. Lett. 121 (19) (2018) 194301, http://dx.doi.org/10.1103/PhysRevLett.121.194301.
[31] J. Li, X. Zhu, C. Shen, X. Peng, S.A. Cummer, Transfer matrix method for the analysis of space-time-modulated media and systems, Phys. Rev. B 100 (14) (2019) 144311, http://dx.doi.org/10.1103/PhysRevB.100.144311.
[32] J. Li, C. Shen, X. Zhu, Y. Xie, S.A. Cummer, Nonreciprocal sound propagation in space-time modulated media, Phys. Rev. B 99 (14) (2019) 144311, http://dx.doi.org/10.1103/PhysRevB.99.144311.
[33] L.L. Foldy, The multiple scattering of waves. I. General theory of isotropic scattering by randomly distributed scatterers, Phys. Rev. 67 (3–4) (1945) 107, http://dx.doi.org/10.1103/PhysRev.67.107.
[34] P.C. Waterman, R. Truell, Multiple scattering of waves, J. Math. Phys. 2 (4) (1961) 512–537, http://dx.doi.org/10.1063/1.1703737.
[35] G. Gaunaurd, H. Überall, Resonance theory of bubbly liquids, J. Acoust. Soc. Am. 69 (2) (1981) 362–370, http://dx.doi.org/10.1121/1.385462.
[36] P.A. Martin, Multiple Scattering: Interaction of Time-Harmonic Waves with N Obstacles, Vol. 107, Cambridge University Press, 2006.
[37] D. Torrent, D. Mayou, J. Sánchez-Dehesa, Elastic analog of graphene: Dirac cones and edge states for flexural waves in thin plates, Phys. Rev. B 87 (11) (2013) 115143, http://dx.doi.org/10.1103/PhysRevB.87.115143.
[38] P. Packo, A.N. Norris, D. Torrent, Inverse grating problem: Efficient design of anomalous flexural wave reflectors and refractors, Phys. Rev. A 11 (1) (2019) 014023, http://dx.doi.org/10.1103/PhysRevApplied.11.014023.
[39] X. Pu, A. Palermo, A. Marzani, A multiple scattering formulation for finite-size flexural metasurfaces, Proc. R. Soc. Lond. Ser. A Math. Phys. Eng. Sci. 478 (2262) (2022) 20210669, http://dx.doi.org/10.1098/rspa.2021.0669.
[40] E. Garova, A. Maradudin, A. Mayer, Interaction of Rayleigh waves with randomly distributed oscillators on the surface, Phys. Rev. B 59 (20) (1999) 13291, http://dx.doi.org/10.1103/PhysRevB.59.13291.
[41] N. Boechler, J. Eliason, A. Kumar, A. Maznev, K. Nelson, N. Fang, Interaction of a contact resonance of microspheres with surface acoustic waves, Phys. Rev. Lett. 111 (3) (2013) 036103, http://dx.doi.org/10.1103/PhysRevLett.111.036103.
[42] A. Maznev, On the effective medium model of the interaction of Rayleigh waves with mass–spring oscillators on the surface, Wave Motion 115 (2022) 103074, http://dx.doi.org/10.1016/j.wavemoti.2022.103074.
[43] A. Karlos, P. Packo, Symmetric flexural wave transmission and linear behaviour in a nonlinear system of two scatterers on a beam, J. Sound Vib. 541 (2022) 117310, http://dx.doi.org/10.1016/j.jsv.2022.117310.
[44] X. Pu, A. Palermo, A. Marzani, Topological edge states of quasiperiodic elastic metasurfaces, Mech. Syst. Signal Process. 181 (2022) 109478, http://dx.doi.org/10.1016/j.ymssp.2022.109478.